Bulletin of the Seismological Society of America. Vol. 65, No. 1, pp. 193–225. February 1975

STRONG GROUND MOTION OF THE SAN FERNANDO, CALIFORNIA, EARTHQUAKE: GROUND DISPLACEMENTS

BY THOMAS C. HANKS

ABSTRACT

Two hundred and thirty-four components of ground displacement are the basis of an investigation of long-period strong ground motion in southern California arising from the San Fernando, California, earthquake. The displacement data are obtained from the double integration of strong-motion accelerograms via the base-line adjustment and filtering operations routinely performed in the series "Strong Motion Earthquake Accelerograms". These procedures can recover long-period data from strong-motion accelerograms with considerable accuracy. Many-station comparisons of displacement data for which the station spacing is small compared to the wavelengths of interest reveal that uncertainties in displacement are less than 1 cm in the period range 5 to 8 sec, 1 to 2 cm at periods near 10 sec, and 2 to 4 cm in the period range 10 to 15 sec, for a data sensitivity of approximately 7.6 cm/g. For limited variations in epicentral distance (R) and source-station azimuth (φ), ground displacements show a strong coherence; for wider variations in R and φ, many of the observed variations in the displacement wave forms are easily attributable to well-understood seismological phenomena. Seismic moment, source dimension, radiation pattern, rupture propagation, the development of surface waves and their subsequent dispersion, and azimuthal variations in the gross geological structure all appear to have first-order significance in fashioning the gross amplitude and frequency content of the displacement wave forms and in explaining observed variations with R and φ. The essential simplicity of these displacement wave forms offers considerable optimism that long-period strong ground motion can be realistically synthesized with advance knowledge of the earthquake source parameters and gross geological structure.

INTRODUCTION

The basis of this study is an investigation of 234 components of ground displacement as a measure of long-period strong ground motion recorded at 78 sites at local distances following the San Fernando, California, earthquake (February 9, 1971; $M_L = 6.4$). The abundance and quality of these data, derived from the double integration of strong-motion accelerograms, provide an unprecedented opportunity to study in detail the source mechanism of this earthquake, to assess the influence of the local crustal structure on the elastic radiation, and thus to develop the embryo of a rational capability to understand and ultimately to synthesize strong ground motion from a damaging and locally destructive California earthquake. Accelerograph site data are presented in Tables 1 to 6; Figure 1 displays the locations of 64 of these 78 sites.

The limitation of the present study to long-period strong ground motion is motivated by the physically plausible proposition that both the source excitation and subsequent modification, due to a heterogeneous propagation medium, of ground-motion amplitudes are progressively simpler, that is, more easily understood, at progressively longer periods. The principal limitation of this approach is the present capability to extract accurate long-period data from the available accelerograms. Within this latter constraint, dis-

placements computed from strong-motion accelerograms are used here as a convenient, physically significant, and sufficiently accurate measure of long-period strong ground motion.

Beyond the problems of accurately recovering long-period strong ground motion, which are discussed in some detail in subsequent sections, an apparent limitation of this approach is that the period range of interest here is somewhat beyond that of normal

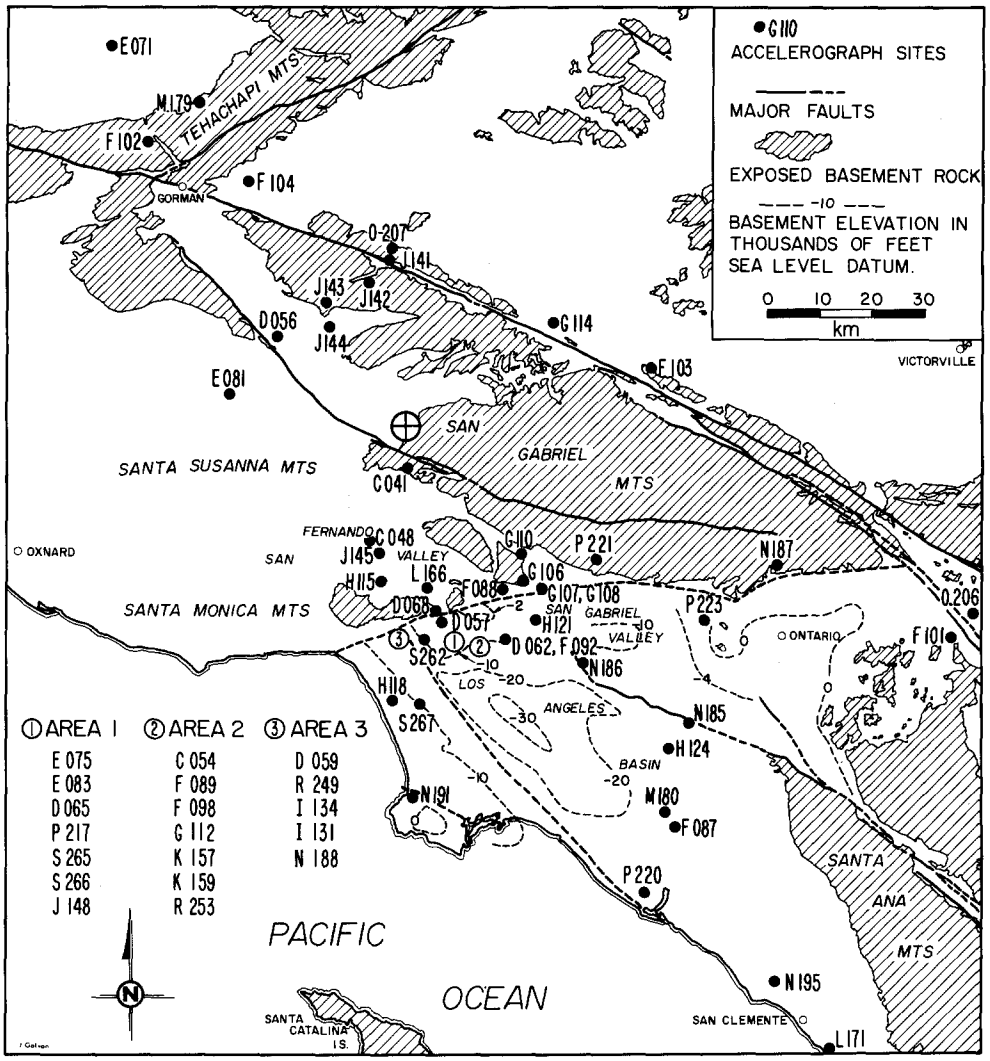

FIG. 1. The site locations of 64 of the 78 accelerographs at which ground displacements are considered in the text are superimposed on the gross geological and structural configuration of the Los Angeles Basin and environs. The encircled cross is the Allen *et al.* (1973) epicenter for the San Fernando earthquake.

engineering significance. Certainly, however, enough structures with fundamental periods of several seconds or greater, including very high buildings, suspension bridges, and large capacity storage tanks, exist such that the results of this study are of more than passing engineering significance. Even so, the particular engineering significance of a given period range is largely beside the point if amplitudes of expected ground motion within it cannot be deterministically understood.

Because of the intrinsic smoothing process of integration and the rudimentary physical proposition mentioned above, the amplitudes of ground displacement should be generated and propagated more coherently than amplitudes of ground velocity and these, in turn, more so than amplitudes of ground acceleration. A comprehensive investigation of strong-motion data of the sort available for the San Fernando earthquake begins quite naturally, then, with ground displacements, as a physically significant, convenient measure of long-period strong ground motion. This lowest common denominator of physical simplicity is an essential feature of this study, since the interpretive framework in which to cast the observations presented here is largely unknown. Many of the observations, and almost all of the high signal-to-noise data, were obtained within several source dimensions of the San Fernando earthquake epicenter. While such distances need not qualify as near-field, it is certainly not obvious that they are far-field, where most seismological experience lies.

Nevertheless, the interpretive framework in which the gross features of the ground displacement data will be cast is largely based on this far-field experience. The parameters and concepts of seismic moment, source dimension, radiation pattern, source propagation, the development of surface waves and their subsequent dispersion, and the local structure of the Los Angeles Basin all, apparently, have first-order significance in the shaping of ground displacement as a function of distance and azimuth. In the absence of detailed numerical calculations, however, there is little basis in fact that this interpretive framework is indeed the correct one, and in any case the observed ground displacements demonstrate a complexity well beyond the first-order nature of this interpretive framework. Surprising or not, it is nevertheless very encouraging that much of the gross structure of long-period strong ground motion recorded at local distances can at least be explained by well understood seismological phenomena, and that this is the case constitutes the primary conclusion of this investigation.

Displacement Data and Long-Period Error Analysis

The ground displacements presented in this paper are derived from the double integration of "corrected" accelerograms via the procedures described by Trifunac (1970, 1971). The corrected accelerogram is obtained from the "uncorrected" accelerogram, i.e., raw acceleration digital data minus the fixed trace digital data, by a series of filtering operations and base-line adjustments; the frequency passband of the corrected acceleration data is displayed in Figure 2. The high-frequency cut off f_{HC} is defined by the temporal spacing of digital points, whereas the low-frequency cut off f_{LC} is defined by the amplitude-frequency characteristics of the long-period noise introduced by the processing techniques. From a largely statistical point of view, Trifunac *et al.* (1973b) have investigated the nature and magnitude of the long-period errors. In terms of "typical" operating and "routine" processing conditions, they cast these results into likely estimates of long-period spectral errors and specified the choice of $f_{LC} = 0.07$ Hz as a frequency below which long-period errors became unacceptably large.

The primary purpose of this section is to evaluate empirically the accuracy of computed displacements by comparing the displacements at a number of stations sufficiently close together that the actual ground displacement at all of them must have been very nearly the same, no matter what the instrument, trigger time, processing technique or initial velocity. As a prelude to these comparisons, we briefly recapitulate the results of Trifunac *et al.* (1973b) and describe some special circumstances of the San Fernando earthquake data to estimate in advance likely errors in computed displacements in a specified period range.

Expected Errors in Ground Displacement

(*a*) *Typical operating and routine processing conditions.* Trifunac *et al.* (1973b) considered five data-sets derived from five independent digitizations of the same straight line; the mean of these data-sets serves as a base line with which to correct the five "accelerograms" for systematic errors of the digitizing machine. With the application of "typical" instrumental operational characteristics (recording speed 1.11 cm/sec, sensitivity 16.5 cm/g, and record length 60 cm) and routine processing conditions (digital capability 312 pts/cm) to these data, individual harmonic amplitudes of the doubly integrated "base line-corrected accelerograms" at periods near 15 sec were approximately 6 mm. (This estimate is obtained from $\tilde{u} = nAT/2$ where $nT = 60$ sec, $A =$ displacement amplitude of a sine wave with period T, and $\tilde{u}$ is the amplitude spectral density of the doubly integrated "base line-corrected accelerograms" at period T; Trifunac *et al.* (1973b) estimated A to be 3 mm with the relation $\tilde{u} = nAT$.) At periods

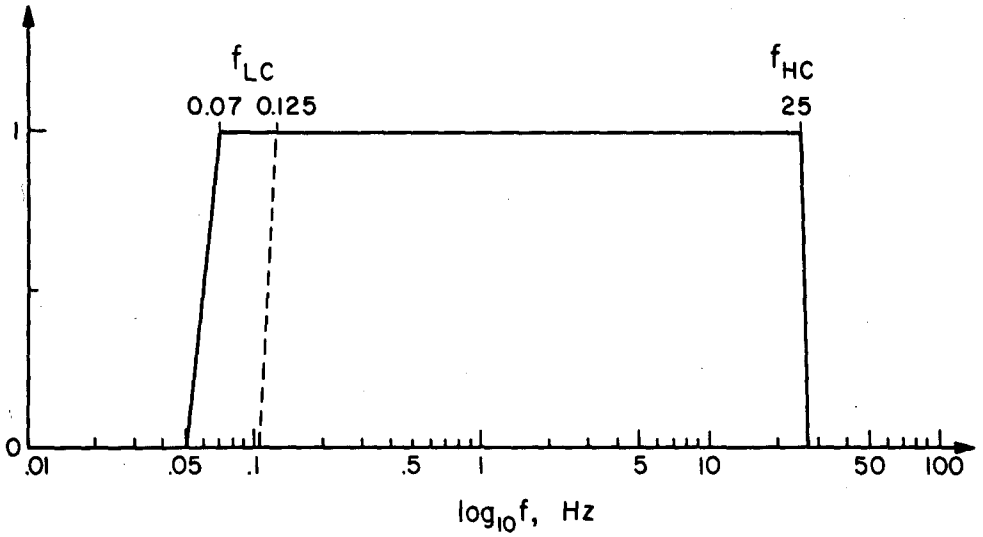

FIG. 2. The frequency passband of the data presented in the series "Strong Motion Earthquake Accelerograms" and of the displacement data considered in the text. The solid line indicates the frequency passband of routinely processed data; the dashed line is employed to eliminate the spurious 11-sec excitation.

near 8 sec this value is approximately 3 mm. The predominant source of this error was the digital capability, i.e., random error corresponding to approximately 1 digital point.

This serves as a minimum error for long-period (5 to 15 sec) displacements, since a general long-period pulse represents a sum over several individual harmonics. The standard deviation of the doubly integrated "acceleration" data is approximately 20 digital points, corresponding to approximately 3 cm of uncertainty in computed displacements. Inasmuch as this function took the approximate form of a step with a several-second rise time, it should be expected to overestimate the error in band-limited displacements. For "routine" processing conditions (for example, the series "Strong Motion Earthquake Accelerograms" prepared by the Earthquake Engineering Research Laboratory of the California Institute of Technology), the frequency-band limit is the solid line of Figure 2. For typical operating and routine processing conditions the error in long-period displacements is bounded by 6 mm and 3 cm and is tentatively estimated here to be 1 to 2 cm.

It is important to recognize the provisional aspects of this error estimate. First, it is based on a record duration of 60 sec. While this is a reasonable estimate of the record length of the older accelerograms (Trifunac, 1970), the number of accelerograms with duration considerably shorter than 60 sec is rapidly increasing, both because different mechanical specifications of available instruments can produce highly variable record lengths for the same earthquake recorded at the same site and because the deployment of closely spaced accelerometer arrays is generating a considerable number of small duration records from small magnitude shocks. The ability to extract accurately long-period information clearly depends on the record length; it is unrealistic to expect accurate 15-sec information from a record less than 30 sec long.

Second, the error estimate is in any case statistical. Errors considerably greater than the above estimate, as well as considerably less, can be expected with a finite probability. This possibility should not be ignored in those investigations, dictated by special site or structural circumstances, which rely wholly or largely on the analysis of a single record. Finally, the exact nature of the error estimate depends on the details of the displacement pulse with which it is associated. The estimate of 1 to 2 cm at long periods is given with the understanding that a general displacement pulse represents more than one individual harmonic but less than a sum over a broad band. In the absence of a more detailed understanding of the expected pulse shape, this estimate is necessarily approximate.

(*b*) *San Fernando earthquake accelerograms.* With respect to the operating and processing conditions assumed in the previous section, accelerograms of the San Fernando earthquake were atypical and nonroutine in two important ways. Both are related to the large number of accelerograms written on 70- and 35-mm film, the first time strong-motion accelerograms were obtained in any substantial number from such accelerograph systems. The first difficulty relates to the low operating sensitivity (approximately 2 cm/g, of the accelerograms written on 70- and 35-mm film, and the second relates to the details of the photographic enlargement effected to offset the first problem.

Both the RFT-250 and SMA-1 accelerograph systems record on 70-mm film at operating sensitivities of approximately 1.9 cm/g for all three components of motion. The MO-2 instrument records on 35-mm film at an operating sensitivity of approximately 2.5 cm/g on the vertical component and 1.5 cm/g on the two horizontal components. The AR-240 accelerograph records on 12-in photographic paper at an operating sensitivity of approximately 7.6 cm/g for all components, whereas the original Coast and Geodetic Survey "standard" accelerographs record on 6-in photographic paper at the "typical" sensitivity of approximately 16 cm/g.

Prior to digitization, RFT-250 and SMA-1 accelerograms were photographically enlarged four times and the MO-2 accelerograms three times. AR-240 and standard accelerograms were processed from contact negatives of the original record. Of the 78 instruments from which ground displacement records presented here are derived, 66 were either the AR-240 (30), RFT-250 (28), or SMA-1 (8) accelerograph systems. The preponderance of data presented in this study, then, was obtained from accelerograms digitized at an effective sensitivity of approximately 7.6 cm/g and about one-half of the "typical" value quoted by Trifunac (1970) as an average sensitivity of the "standard" accelerograms then available. Other factors being equal (see below), this difference means that the uncertainty in long-period displacements is twice as large as that given in the last section, i.e., 2 to 4 cm at periods near 15 sec. Uncertainties in long-period displacements derived from the six MO-2 accelerographs are expected to be somewhat larger, whereas these uncertainties will be those estimated in the previous section for data obtained from the six "standard" accelerograms.

The process of photographic enlargement also increases the apparent operating speed and total length of record (in centimeters) by the same amount it increases the effective sensitivity. The first two effects should cancel each other with respect to long-period error estimates, provided the actual operating speed is near 1 cm/sec, the actual time length of record is approximately 60 sec, and the temporal spacing of digital points is constant. For most of the San Fernando earthquake accelerograms, these stipulations are met, but some care should be exercised in the dozen or so records of the entire data-set that are less than 30 sec long.

To achieve the 4× photographic enlargement of the accelerograms originally written on 70-mm film, individual 11-sec sections, with a 1-sec overlap, were enlarged separately. Thus the photographic enlargement of the 70-mm film records introduced inherent data discontinuities, as well as effective operating conditions different from the "typical." Because of the relative photographic distortion of adjacent sections, discontinuities of all orders in the time series should be expected to arise, producing spurious excitation at periods $11n$ and $11/n$ sec where n is an integer. Because the routine processing techniques ($f_{LC} = 0.07$ Hz) remove all harmonics with periods greater than 20 sec, the anomalous excitation should be largely confined to periods in the vicinity of 11 sec, the lowest order harmonic present in the routinely processed data. The amplitude of this anomalous excitation is more difficult to predict. It can be expected to depend on the magnitude of the photographic distortion at the end of one section relative to the beginning of the next, the relative distortion between acceleration and fixed traces, the number and positioning of fixed traces, the care with which individual traces are aligned by the operator, and the record length.

Hanks (1973) discussed this problem in some length, and the reader is referred there for details. For the series "Strong Motion Earthquake Accelerograms," all 70- and 35-mm film records of the San Fernando earthquake were reprocessed with the frequency passband given by the dashed lines of Figure 2 (Trifunac *et al.*, 1973a); this passband removes contributions from all periods greater than 10 sec. In the interest of data uniformity necessary for this investigation, *all* displacement records presented here have been processed with this passband ($f_{LC} = 0.125$ Hz), with the exception of three sets of displacement records, noted explicitly, used to illustrate the anomalous 11-sec excitation and the general magnitude of the long-period errors.

In subsequent discussions, the term long-period strong ground motion thus refers to the band from the shortest periods discernibly present in the displacement wave forms, generally between 1 to 2 sec, and 8 to 10 sec. At periods near 8 sec, the results of Trifunac *et al.* (1973b) suggest that the uncertainty in displacements should be 1 cm or so, for an effective sensitivity of 7.6 cm/g appropriate to the bulk of the San Fernando earthquake accelerograms. In the next section, this error estimate is empirically evaluated with computed displacement records.

Comparisons of Closely Spaced Ground Displacements

If a set of stations is spaced at distances small compared to the wavelengths of a frequency band of interest and if the variation of material properties is not appreciable within the immediate vicinity of the array, there should be little distortion of a long-period disturbance as it crosses the array. For example, for periods of 3 to 4 sec and greater with wavelengths of approximately 10 km or longer, there should be little distortion of signal amplitudes across an array of the dimension of 1 to 2 km or less. In the limit of infinitesimal station spacing, this correlation must be exact. Any differences in long-period amplitudes must then be attributed to instrumental or processing errors.

Figure 3 locates instrumental sites in four area groups for which the station spacing is extremely small. Stations are identified with the referencing system of the series "Strong Motion Earthquake Accelerograms" being prepared by the Earthquake Engineering Research Laboratory of the California Institute of Technology; that is, the accelerogram obtained from the site labeled J148 (Area 1) is the 148th entry of this series and appears in Part J. In the displays of computed displacements, these identifications are prefixed with

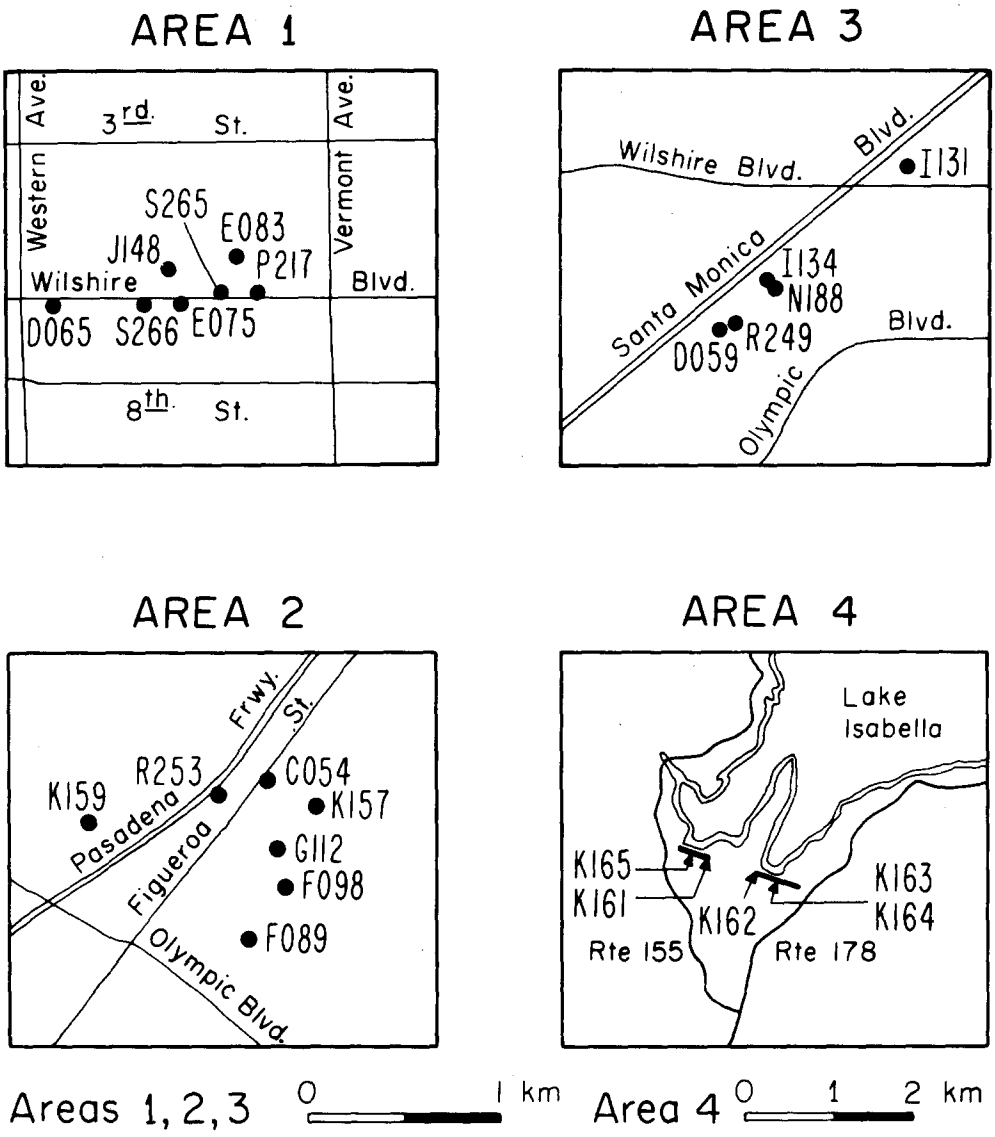

FIG. 3. Accelerograph site locations for Areas 1, 2, 3, and 4.

the Roman numeral II, indicating Volume II (corrected accelerograms, velocities, and displacements) processing.

Three components of displacement are presented for the sites of Area 1 in Figure 4A (f_{LC} = 0.07 Hz) and Figure 4B (f_{LC} = 0.125 Hz); three components of displacement are presented for the sites of Area 2 in Figure 5 (f_{LC} = 0.125 Hz). Figure 6A (f_{LC} = 0.07 Hz) and Figure 6B (f_{LC} = 0.125 Hz) present these data for Area 3. In Figure 7, three components of displacement are presented for the five sites on Lake Isabella Dam for

three different low cut-off frequencies (f_{LC} = 0.100, 0.125, and 0.167 Hz). Table 1 summarizes site address and instrument location, instrument type, record length and building height data pertinent to the sites and records of the four area groupings. Epicentral distances (R) and source-station azimuths (φ) for these area groupings are given with respect to the epicenter of Allen *et al.* (1973). For all sites in all areas, the computed displacements are regarded as actual ground displacements, contaminated to some extent by processing-generated noise and, in the few cases for which instrumental locations were above the ground level, by structural vibrations. Given the period range of interest here and the heavy reliance on basement, ground level, or free-field sites, contamination

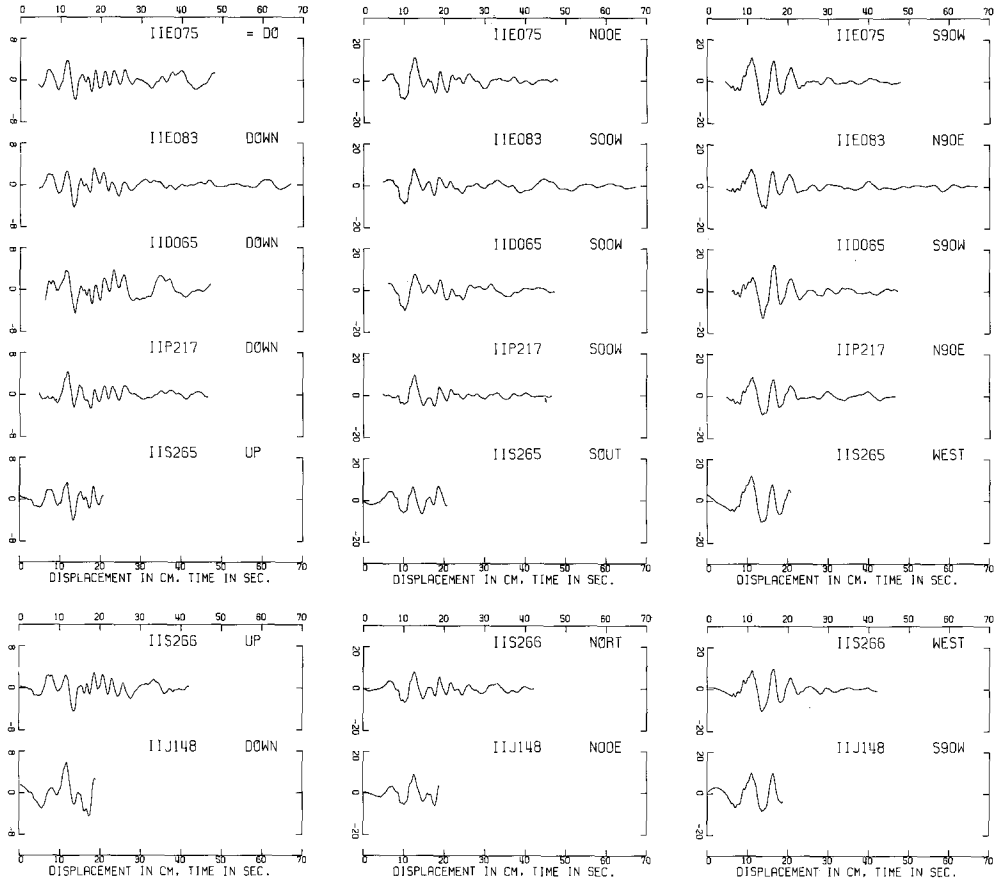

FIG. 4A. Ground displacements in Area 1 (f_{LC} = 0.07 Hz).

by structural response is not an important problem, as will be seen shortly, although there is occasional evidence for its presence [e.g., one horizontal component at K159 (Figure 5) and all components of motion at F088 (Figure 10A)].

To make detailed comparisons of the computed ground displacements, it is necessary to provide a common orientation of the three components of motion and a common time base for all of the sites within any area. In Area 4, all instrumental axes were aligned in the same direction, and in Area 1 all instrumental axes were oriented in either the north-south or east-west directions. In the other two areas, the horizontal axes are approximately, but not exactly aligned along two orthogonal directions. Beyond providing the appropriate polarity changes, it is necessary only to be alert for component misidenti-

fications, relative to the actual orientation of the instrumental axes, several of which are noted below.

In Area 4, all instruments were interconnected with a common triggering facility, but in Areas 1, 2 and 3, instruments at each site were triggeredin dependently. To provide the necessary common time bases for the records of these three areas, a high-frequency, predominantly horizontal arrival (*S*!) was read on the acceleration and velocity traces for each station; displacement records in any one area were then aligned with respect to this arrival, since the dimension of any area grouping is sufficiently small that the transit time of this (presumably shear) arrival across it should be no more than several

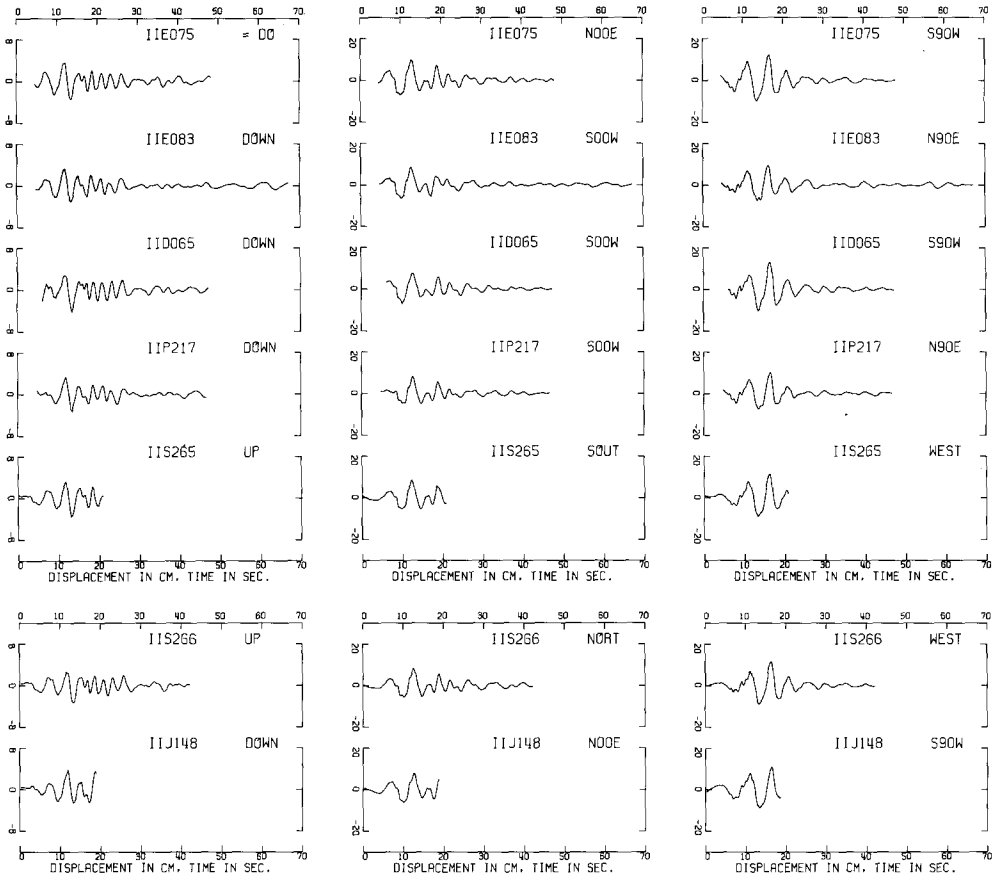

FIG 4B. Ground displacements in Area 1 (f_{LC} = 0.125 Hz).

tenths of a second. The high-frequency character of *S*! allows for an accurate estimate of its arrival time (±0.2 sec); examples of *S*! for areas 1, 2, and 3 are displayed in Figure 8. *S*! is only barely discernible, if at all, upon double integration to obtain the computed displacements; it thus provides a common time base largely independent of the much longer-period displacements.

Area 1 (Figure 4, A and B). The displacement records at the seven sites of Area 1 have been temporally shifted such that *S*! arrives at 6.4 sec for all components. Ground displacements in the vertically upward, north, and east directions are along the positive ordinates of the left, middle, and right columns of Figure 4, A and B irrespective of the indicated components of motion. These values define directions of motion relative to the

instrumental axis orientation; inasmuch as they represent the only component identification in the data format of "Strong Motion Earthquake Accelerograms," they are retained in these displays as basic identification data.

On the east component S! is discernible as a relatively small, high-frequency precursor to the large amplitude, long-period displacements arriving between 7 and 20 to 25 sec. On the up and north displacements, it is only barely discernible. For each component of motion, these long-period arrivals at each site have been very precisely aligned in time by the temporal shift based on S!.

In Figure 4A (f_{LC} = 0.07 Hz), the agreement between the east components of motion is particularly good. Three large amplitude peaks arrive between 10 and 22 sec; both

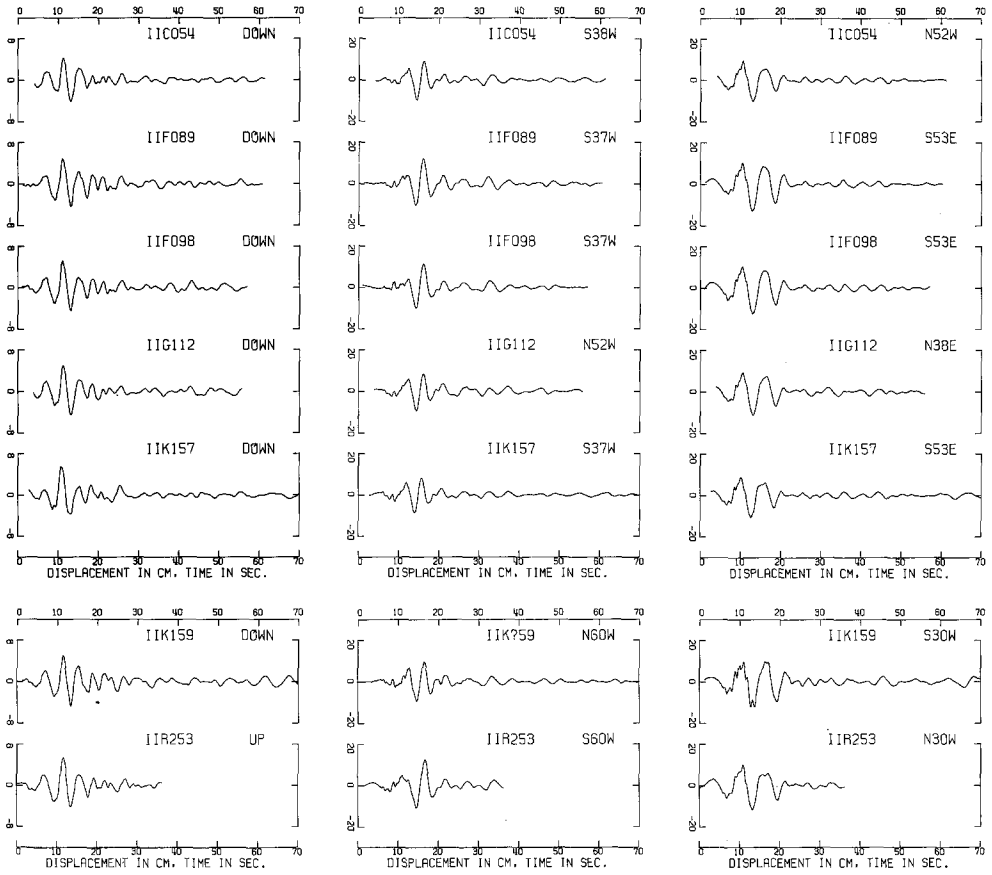

FIG. 5. Ground displacements in Area 2 (f_{LC} = 0.125 Hz).

the arrival times and displacement amplitudes compare well. Beyond 30 sec, however, noncorrelatable arrivals with amplitudes of several centimeters are present. Relative long-period distortion of the main energy group on the north component of motion is apparent, and on the vertical component the relative long-period distortion of the main energy group is even more severe, but this appearance is largely due to the smaller displacements on the vertical component of motion.

In Figure 4B (f_{LC} = 0.125 Hz), the agreement between the computed displacements for each component of motion at the seven sites of Area 1 is considerably better, although the basic shape of the main energy group is essentially unchanged (e.g., east component, Figure 4, A and B). Within the context of this comparative analysis, it is difficult to

understand why energy in the period range of several to 8 sec would be more coherent than energy at longer periods. The obvious conclusion is to associate the relative long-period distortion and noncorrelatable phases of Figure 4A to errors in the determination

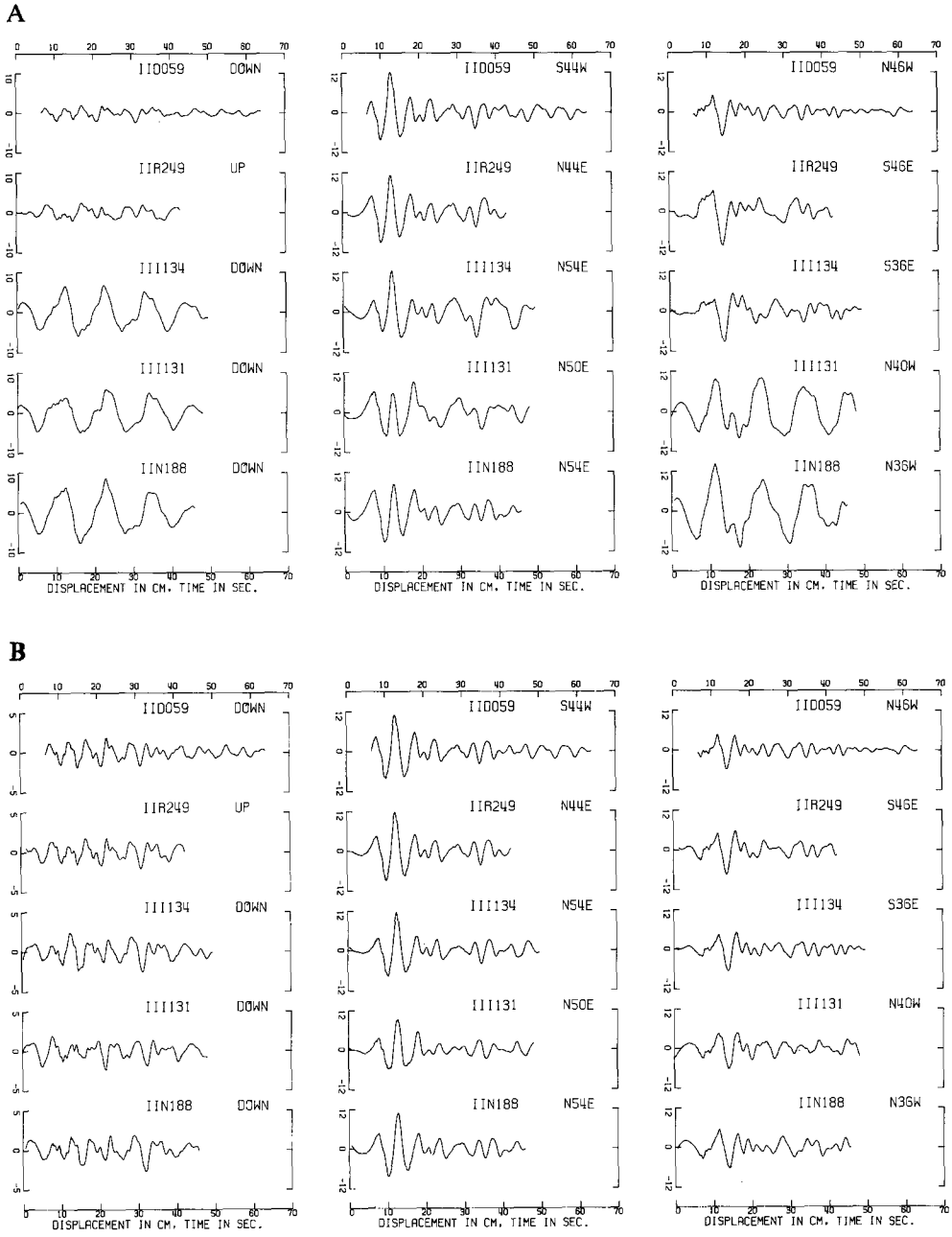

FIG. 6. Ground displacements in Area 3: A, $f_{LC} = 0.07$ Hz; B, $f_{LC} = 0.125$ Hz.

of long-period (10 to 15 sec) displacements. For an effective sensitivity of 7.6 cm/g, this period range should contribute uncertainties of several centimeters to the computed displacements. The removal of these contributions in Figure 4B allows relatively small (amplitudes < 2 cm) arrivals to be discerned and correlated as much as 35 to 40 sec after

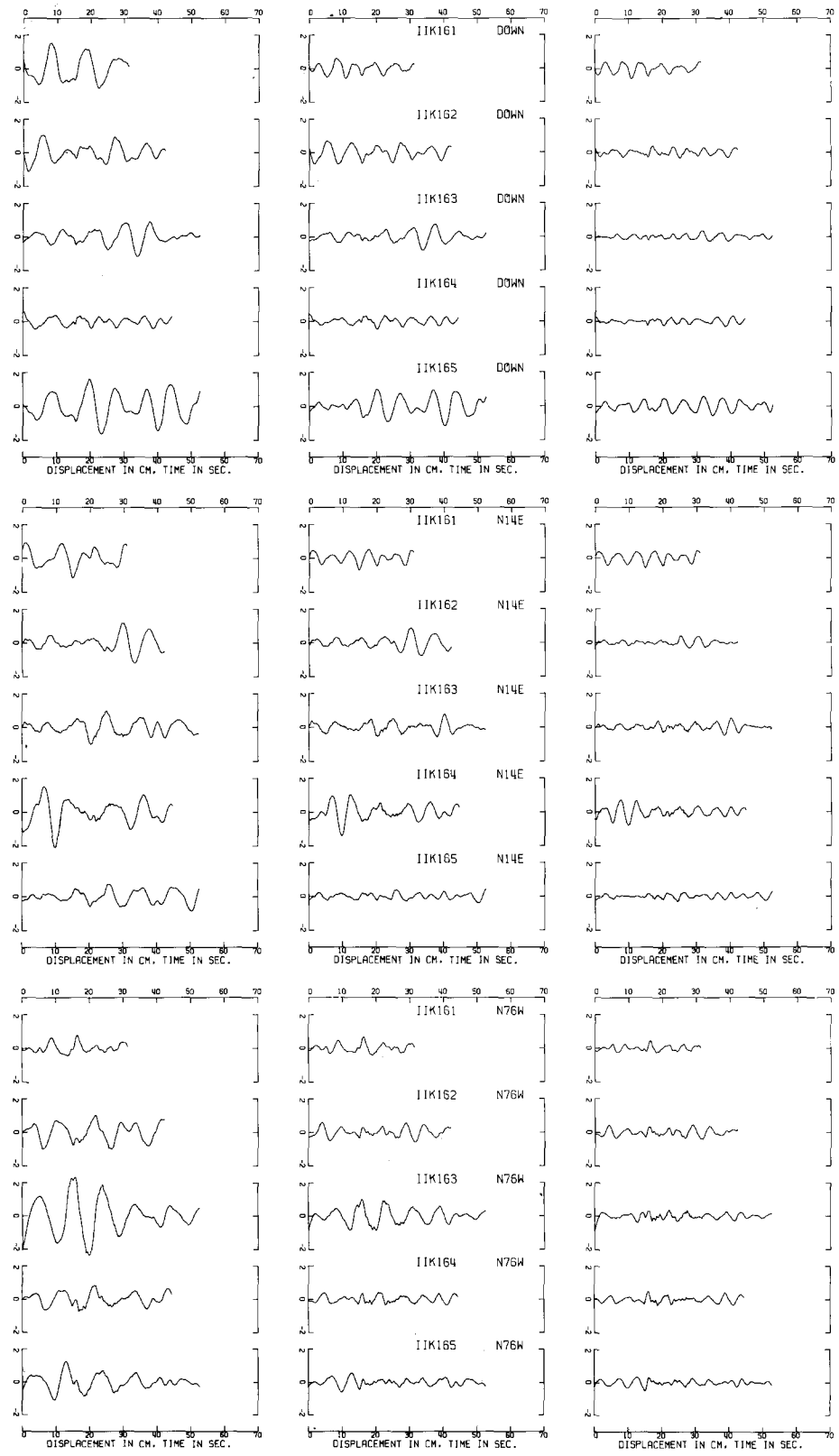

FIG. 7. Ground displacements in Area 4: $f_{LC} = 0.100$ Hz in left column, $f_{LC} = 0.125$ Hz in middle column, $f_{LC} = 0.167$ Hz in right column.

first motion (e.g., north component, Figure 4B). Most of the relative distortion of the main energy group between 7 and 20 to 25 sec has been removed.

Indeed, the agreement between sites for each component of ground displacement is quite good; the displacements are not noticeably influenced by instrumental type, record length, building height, or triggering time, within the available variations of these parameters. At the sensitivity of these data, the statistical error analysis of Trifunac *et al.*

TABLE 1

STATION DATA

EERL-CIT Ref. No.	Address and Location	Instrument	Record Length (sec)	Building Height (stories)
	Area 1: $R = 40$ km, $\varphi = 167°$			
E075	Los Angeles, 3470 Wilshire, sub-bsmt.	AR-240	44	11
E083	Los Angeles, 3407 W. Sixth, bsmt.	AR-240	62	7
D065	Los Angeles, 3710 Wilshire, bsmt.	AR-240	41	11
P217	Los Angeles, 3345 Wilshire, bsmt.	AR-240	42	12
S265	Los Angeles, 3411 Wilshire, 5th bsmt.	MO-2	21	31
S266	Los Angeles, 3550 Wilshire, bsmt.	MO-2	42	21
J148	Los Angeles, 616 S. Normandie, bsmt.	SMA-1	18	17
	Area 2: $R = 42$ km, $\varphi = 161°$			
C054	Los Angeles, 445 S. Figueroa, sub-bsmt.	AR-240	57	39
F089	Los Angeles, 808 S. Olive, grd. lvl.	AR-240	60	8
F098	Los Angeles, 646 S. Olive, bsmt.	AR-240	56	8
G112	Los Angeles, 611 W. Sixth, bsmt.	RFT-250	52	43
K157	Los Angeles, 420 S. Grand, 2nd fl.	RFT-250	85	16
K159	Los Angeles, 750 S. Garland, 2nd fl.	RFT-250	94	8
R253	Los Angeles, 533 S. Fremont, bsmt.	MO-2	36	10
	Area 3: $R = 39$ km, $\varphi = 186°$			
D059	Los Angeles, 1901 Ave. of Stars, sub-bsmt.	AR-240	57	19
R249	Los Angeles, 1900 Ave of Stars, bsmt.	MO-2	41	27
I134	Los Angeles, 1800 Century Park East, bsmt.	SMA-1	49	15
I131	Beverly Hills, 450 N. Roxbury, 1st fl.	SMA-1	48	10
N188	Los Angeles, 1880 Century Park East grd. lvl.	SMA-1	45	16
	Area 4: $R = 137$ km, $\varphi = 357°$			
K161	Lake Isabella Dam, gallery	RFT-250	31	
K162	Lake Isabella Dam, auxiliary abutment	RFT-250	42	
K163	Lake Isabella Dam, auxiliary crest	RFT-250	53	
K164	Lake Isabella Dam, control tower	RFT-250	45	
K165	Lake Isabella Dam, crest	RFT-250	53	

(1973b) would suggest displacement uncertainties of approximately 1 cm in the period range near 8 sec; the displacements of Figure 4B are in reasonable accord with this expectation.

Area 2 (Figure 5). The displacement records at the seven sites of Area 2 have been temporally shifted such that S! arrives at 5.9 sec. Ground displacement vertically upward, to the northeast, and to the southeast are along the positive ordinates of the left, middle, and right columns, respectively, of Figure 5. For the first five sites of Area 2 (C054, F089, F098, G112, and K157), the instrumental axes are well-aligned; that is, in

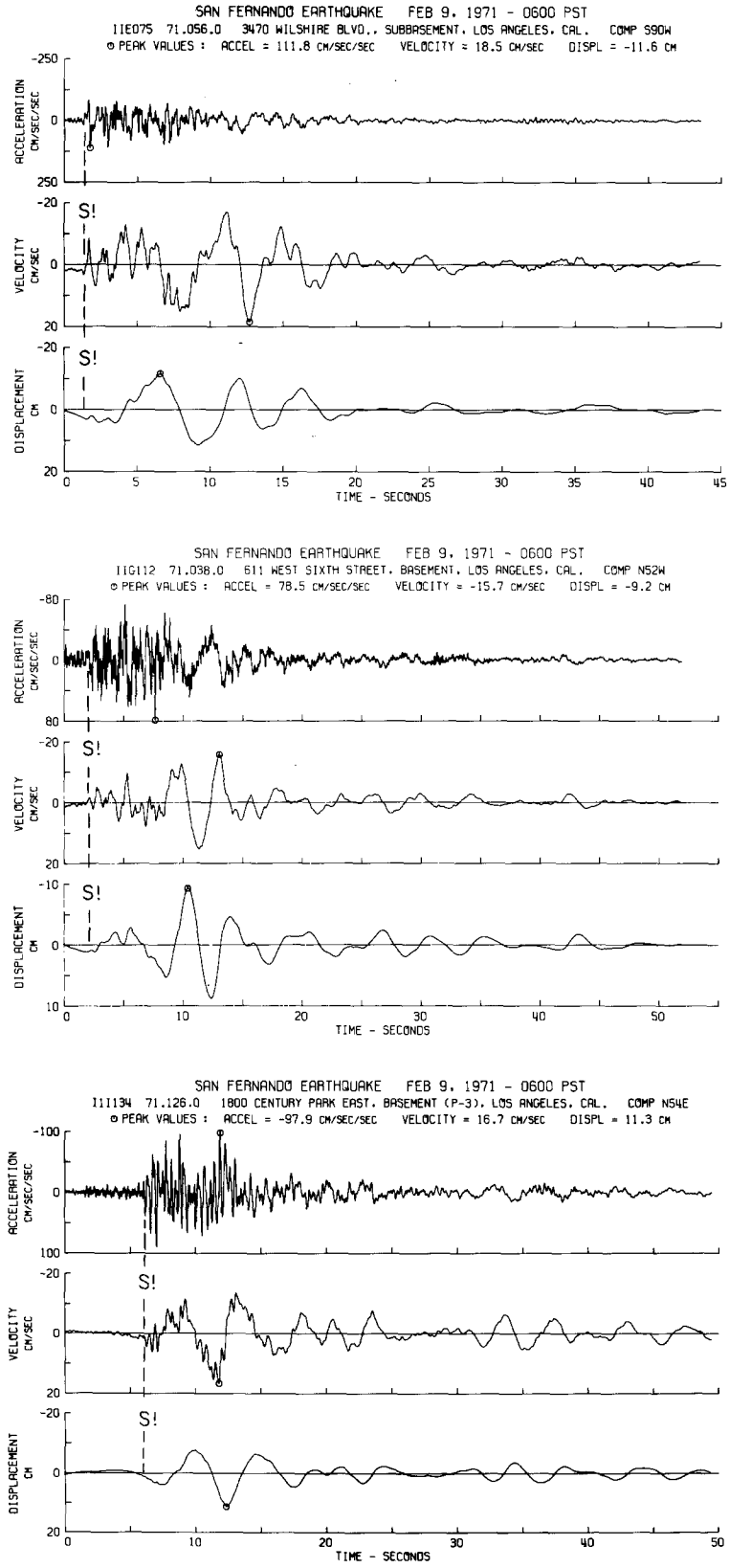

FIG. 8. Acceleration, velocity, and displacement for one component of ground motion at one site of Area 1 (*top*), one site of Area 2 (*middle*) and one site of Area 3 (*bottom*) with the identification of *S*!

the southeast direction, ground displacements are in the S 53°E or S 52°E directions. The instrumental axes at K159 and R253 are not so conveniently aligned; in the southeast directions S 60°E is recovered at K159 and S 30°E at R253. Component misidentifications at G112 and K159 were detected and confirmed; the component of motion labeled N38E is in fact the N52W component of motion at G112, and conversely. Similarly, the component of motion labeled S30W is in fact the N60W component of motion at K159.

The amplitudes, frequency content, and arrival times of the main energy group between 7 and 20 to 25 sec agree well for all components of motion, particularly for the first five sites. Discernible and correlatable phases with amplitudes of less than 2 cm can be seen on both horizontal components at 45 to 50 sec, well after the arrival of the main energy group. Coherence on the vertical component is not quite so strong, but the signal strength is considerably weaker. The components of ground displacement at K159 and R253 agree well with the appropriate components of motion elsewhere in Area 2, despite the difference in orientation of components. The ground displacements in Area 2 have broadly the same frequency and amplitude content as in Area 1 (Figure 4B), although the horizontal components of ground displacement are rotated approximately 45° with respect to Area 1. With respect to the accuracy of these ground displacements, the same conclusions reached for Area 1 on the basis of Figure 4B apply to the ground displacements for Area 2 presented in Figure 5.

Area 3 (*Figure 6, A and B*). The displacement records at the five sites of Area 3 have been temporally shifted such that *S*! arrives at 6.4 sec. Ground displacement vertically upward, to the northeast (N44–54E), and to the southeast (S36–46E) are along the positive ordinates of the left, middle, and right columns, respectively. In Figure 6A ($f_{LC} = 0.07$ Hz) the vertical component of displacement at I134, I131, and N188 is dominated by sinusoids of approximately 11-sec period. They have little in common with the smaller amplitude, higher-frequency vertical displacements at D059 and R249. The 11-sec disturbance is also affecting the horizontal components of ground displacement at I134, I131, and N188, although to a more variable extent.

The records obtained at I134, I131, and N188 were all written on 70-mm film, and their processing was subject to the difficulties discussed previously and in Hanks (1973). Indeed, it was comparisons of this sort that led to the identification of this data-processing problem. The most simple expedient to resolve this problem, and the one employed subsequently in this paper, is to use the $f_{LC} = 0.125$ Hz high-pass filter. The application of this filtering operation results in the ground displacements in Area 3 presented in Figure 6B. The agreement between the ground displacements at the five sites for each component of motion has been considerably improved.

The amplitudes of the vertical component of ground displacement are considerably less than those observed in Areas 1 and 2. Even though maximum amplitudes of vertical ground displacement are less than 2 to 3 cm, discernible phases are present at all sites at the same times, although details of the correlation are not so clear. Correlation of phases on the horizontal components is more easily definable, primarily because of the larger amplitude of the ground displacements.

Area 4 (*Figure 7*). Three components of ground displacement are presented for the five sites on Lake Isabella Dam in Figure 7. Displacements are presented for three different selections of f_{LC}: $f_{LC} = 0.100$ Hz in the left column, $f_{LC} = 0.125$ Hz in the middle column, and $f_{LC} = 0.167$ Hz in the right column. The coherence criterion indicates that virtually all of the displacements in Figure 7 are processing-generated noise, although a high-frequency arrival at approximately 17 sec with amplitude of several millimeters is discernible (e.g., N76W, $f_{LC} = 0.167$ Hz). Figure 7 clearly indicates how uncertainties in ground displacement increase as the maximum period of admitted displacements

increases. In the left-hand column, where periods of 10 to 12 sec are admitted, the processing techniques generate 2 cm of noise. For periods up to 8 to 10 sec (middle column), displacement uncertainties of approximately 1 cm are present, and for periods up to 6 to 7 sec (right column), displacement uncertainties are approximately 5 mm or less. The sensitivity of these data in the form to be digitized was approximately 7.6 cm/g.

All of the accelerograms in Area 4 were written on 70-mm film. The $f_{LC} = 0.100$ Hz filter should pass the 11-sec disturbance at approximately 50 per cent of its actual amplitude. As such, it should not be expected to dominate the $f_{LC} = 0.100$ Hz displacements, although there is occasional evidence for its presence. It is interesting that several of the noncorrelatable phases for the $f_{LC} = 0.167$ Hz displacements consist of sinusoids with a period of approximately $5\frac{1}{2}$ sec. This would be the first higher mode of the spurious 11-sec disturbance, with a predictably smaller amplitude. In the case of the five 70-mm film records of area 4, its amplitude is approximately 5 mm or less.

Summary Discussion of Long-Period Errors

The primary purpose of this comparative analysis of ground displacements is to assess the accuracy with which displacements can be recovered via the procedures utilized in the series "Strong Motion Earthquake Accelerograms". Apart from the 11-sec disturbance arising from the processing of 70-mm film records, the displacement comparisons presented previously suggest that displacement uncertainties are approximately 0.5 to 1 cm in the period range 5 to 8 sec, 1 to 2 cm in the period range 8 to 10 sec, and several (2 to 4) centimeters in the period range of 10 to 15 sec. Almost all of the accelerograms in Areas 1 to 4 were processed at an effective sensitivity of approximately 7.6 cm/g. Corrected for the sensitivity difference, these results are in reasonable accord with the displacement uncertainties expected by Trifunac *et al.* (1973b), on the basis of statistical analysis. The coincidence of these results supports the claim of Trifunac *et al.* (1973b) that the major source of error in the recovery of long-period information from strong-motion accelerograms is the random errors introduced in the digitizing process. The uncertainties in displacement are not a discernible function of instrument type, record length, trigger time or initial conditions.

The spurious 11-sec disturbance was a problem previously unencountered in the series "Strong Motion Earthquake Accelerograms". In that series, this difficulty will be circumvented with the use of the $f_{LC} = 0.125$ Hz high-pass filter for all 70- and 35-mm film records. The same expedient will be used for all records in the remainder of this paper. The 11-sec contribution is formally removed, and the amplitudes of the higher harmonics are not a major source of error.

With the use of the $f_{LC} = 0.125$ Hz high-pass filter, the level of noise in the ground displacements presented in the remainder of this paper is considered to be 1 cm, that estimated for periods near 8 sec.

Ground Displacement Wave Forms and Their Interpretation

The primary consideration of this section is to emphasize the general coherence of ground displacements within limited ranges of epicentral distance and azimuth and to discuss the observed variations of these wave forms over broader ranges of epicentral distance and azimuth in terms of wave propagation effects and various properties of the source mechanism. Even in the absence of formal numerical models, a consideration of such parameters and concepts as seismic moment, source dimension, radiation pattern, source propagation, the development of surface waves and their subsequent dispersion, and gross differences in geological structure as a function of azimuth provides the basis

for understanding the gross amplitude and frequency content of the observed displacement wave forms and their variations with distance and azimuth. This understanding, in turn, enhances the actual significance and coherence of the displacement wave forms, at least from a conceptual point of view, and will provide the basic structure within which to generate synthetic ground displacements.

Area 1 (*Figures 4B and 9*). Figure 9 presents the results of summing the displacement records for each component at sites E075, E083, D065, P217, and S266 in the time interval 6.4 to 40 sec and dividing by 5, with a nominal reduction in the long-period processing-generated noise of a factor of $\sqrt{5}$. The ordering of arrivals according to decreasing period that is clear on all three components of motion suggests the influence of surface-wave dispersion. Since Area 1 is almost due south of the epicenter ($\varphi = 167°$), the east component is essentially the component of transverse motion and is, apparently, primarily comprised of a dispersed Love-wave train. Similarly, the north and vertical components of ground displacement are primarily comprised of a dispersed Rayleigh-wave train. That dispersion of this sort should occur at an epicentral distance (38 km) no greater than several wavelengths of the dispersed arrivals is a significant result with respect to the development of long-period strong ground motion at local distances within the Los Angeles Basin. In view of the depth of low-velocity sedimentary cover in this area of Los Angeles (Figure 1), with the implication of relatively steep material velocity gradients, this result, however, is not totally unexpected.

Following the longer-period arrivals between 5 and 15 sec, a four-peak group of 2 to 3-sec waves is particularly clear on the vertical component between 17 and 27 sec. This group of waves is discernible on the north component, but does not appear to affect the east component. Since this group is primarily confined to the vertical ~ radial plane of motion, it evidently consists of short-period Rayleigh waves significantly delayed from the longer-period motion arriving earlier.

In the *bottom* part of Figure 9, the vertical displacement is plotted as a function of the north-south (~ radial) displacement, with time as a parameter; the letters correspond to points in time indicated in the *top* part of Figure 9. To a large extent, the particle motion trajectories in the *lower* part of Figure 9 are retrograde ellipses typical of Rayleigh waves. The elongation of these ellipses in the radial direction suggests low material velocity in the layers supporting this motion relative to the material velocity of the substratum (Lee, 1932).

In sum, the retrograde elliptical particle motion, the elongation of these ellipses in the radial direction, and the ordering of arrivals according to decreasing period strongly suggests that ground displacements on the vertical and north-south components are largely comprised of Rayleigh waves traversing a region with material properties rapidly increasing with depth as would be expected in this area of Los Angeles. Similarly, the east component of ground displacement consists primarily of a Love-wave train, the dispersion of which is related to the same cause.

Profile 1 (*Figure 10, A and B*). The remainder of the ground displacements in this paper are presented in the form of vertical, radial, and transverse components of motion. Positive vertical motion is in the upward direction, positive radial motion is in the direction radially away from the earthquake epicenter, and positive transverse motion is normal to the positive radial motion in the counterclockwise direction.

Profile 1 consists of 18 stations in a direction southeast from the epicenter. Source-station azimuths vary from 136° to 155°; 12 of the stations are in the range $136 \leqq \varphi \leqq 146°$. Epicentral distances range from 32 to 222 km. Station data for Profile 1 are presented in Table 2, and ground displacements for these sites are presented in Figure 10, A and B.

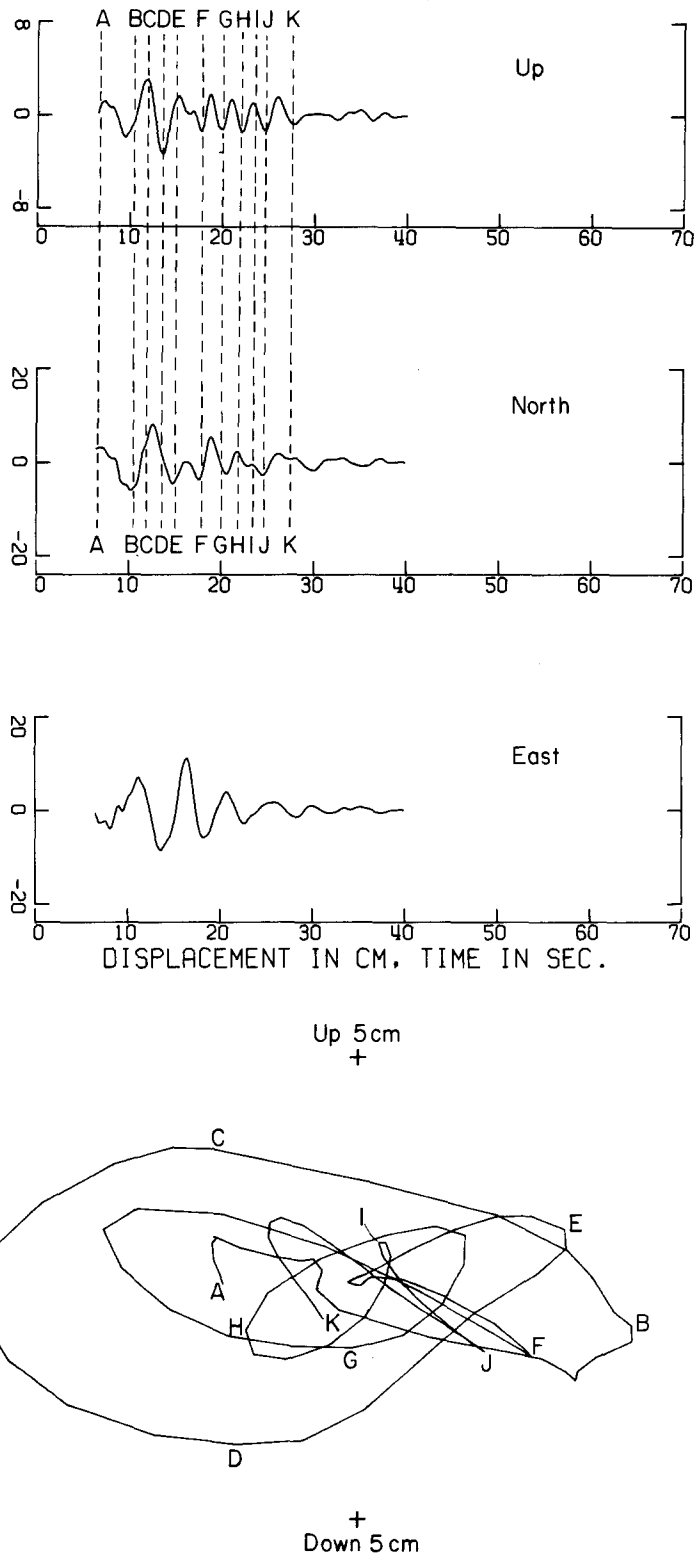

FIG. 9. Three components of averaged ground displacement in Area 1 (*top*). Particle motion trajectories in the vertical-approximately radial plane (*bottom*), the letters parameterizing time.

The phase $S!$ is again the means of temporally aligning the displacement wave forms. Physically, the data have been aligned such that $S!$ is assigned an infinite phase velocity with an arrival at 9.7 sec in Figure 10. At G106 (the Seismological Laboratory of the California Institute of Technology) a comparison of the ground acceleration, velocity, and displacement obtained from the strong-motion accelerograph with the same quantities obtained from the low-gain (4×) Wood-Anderson seismograph, a continuously operating, time-calibrated system, reveals that $S!$ at G106 arrives at 1400:53.5 GMT. On the basis of the $S!-P$ time observed on the Wood-Anderson instrument, $S!$ corresponds to a direct shear arrival from the hypocentral region. Its arrival 1 to 2 sec prior to the larger amplitude, longer-period shear displacements discussed both above and below suggests its origin lies in an event just prior to more massive faulting in the hypocentral region. This inference is suggested by teleseismic observations as well (D. V. Helmberger, personal communication).

TABLE 2

STATION DATA: PROFILE 1

EERL-CIT Ref. No.	Address and Location	Instrument	R (km)	φ (deg)
G110	Pasadena, Jet Propulsion Laboratory, bsmt.	RFT-250	32	137
F088	Glendale, 633 E. Broadway	AR-240	38	149
G106	Pasadena, C.I.T. Seismological Laboratory	RFT-250	36	143
G108	Pasadena, C.I.T. Millikan Library, bsmt.	RFT-250	39	140
G107	Pasadena, C.I.T. Athenaeum	SMA-1	40	139
D062	Los Angeles, 1640 Marengo, 1st fl.	AR-240	43	155
F092	Los Angeles, 2011 Zonal, bsmt.	AR-240	43	154
H121	Alhambra, 900 S. Fremont, bsmt.	SMA-1	43	146
N186	Whittier Narrows Dam	RFT-250	54	143
N185	Brea, Carbon Canyon Dam	RFT-250	75	136
H124	Fullerton, 2600 Nutwood, bsmt.	SMA-1	76	141
M180	Orange, 4000 W. Chapman, bsmt.	RFT-250	84	146
F087	Santa Ana, Engineering Bldg.	Standard	88	146
P220	Costa Mesa, 666 W. 19th	AR-240	96	153
N195	San Juan Capistrano	RFT-250	122	146
L171	San Onofre, Nuclear Power Plant	AR-240	139	146
H127	San Diego, Gas & Electric Bldg., bsmt.	Standard	220	148
P227	San Diego, Light & Power Bldg., bsmt.	RFT-250	222	148

Of the 18 stations of Profile 1, $S!$ was identifiable at all but four (F087, P220, H127, and P227), where it was presumed to have triggered the accelerograph. Three examples and one nonexample (P220) of $S!$ are displayed in Figure 11.

At close ranges ($R \leq 50$ km), $S!$ is the direct shear wave traveling through the upper crust. For greater distances ($70 \leq R \leq 120$ km), $S!$ travels through the lower crust, sampling higher material velocities, and experiences greater amplitude attenuation corresponding to its greater travel path. $S!$ was not identifiable at F087 ($R = 88$ km) and P220 ($R = 96$ km), although it is likely that $S!$ triggered the accelerograph in the latter case (Figure 11). For $R \gtrsim 120$ km, $S!$ will arrive first as an arrival refracted from the Mohorovičić discontinuity, a more efficient propagation path than those for which R is just less than 120 km; the strength of $S!$ at N195 ($R = 122$ km) compared to P220 provides evidence of this. As the phase S_n, $S!$ travels at considerably larger velocities than as the crustal phase S_g.

Because the velocity at which $S!$ travels is a function of R, the expedient of timing the displacement wave forms with the $S!$ arrival has validity only for limited variations of R.

In the absence of detailed knowledge of the travel path characteristics of $S!$, this expedient will not allow any quantitative conclusions to be drawn about crustal structure from the relative arrivals of the other phases.

The first nine stations of Profile 1 (Figure 10A) are at epicentral distances of 32 to 54 km. The displacement wave forms, as aligned on the basis of $S!$, show a strong coherence in Figure 10A, with subtle but real variations with increasing epicentral dis-

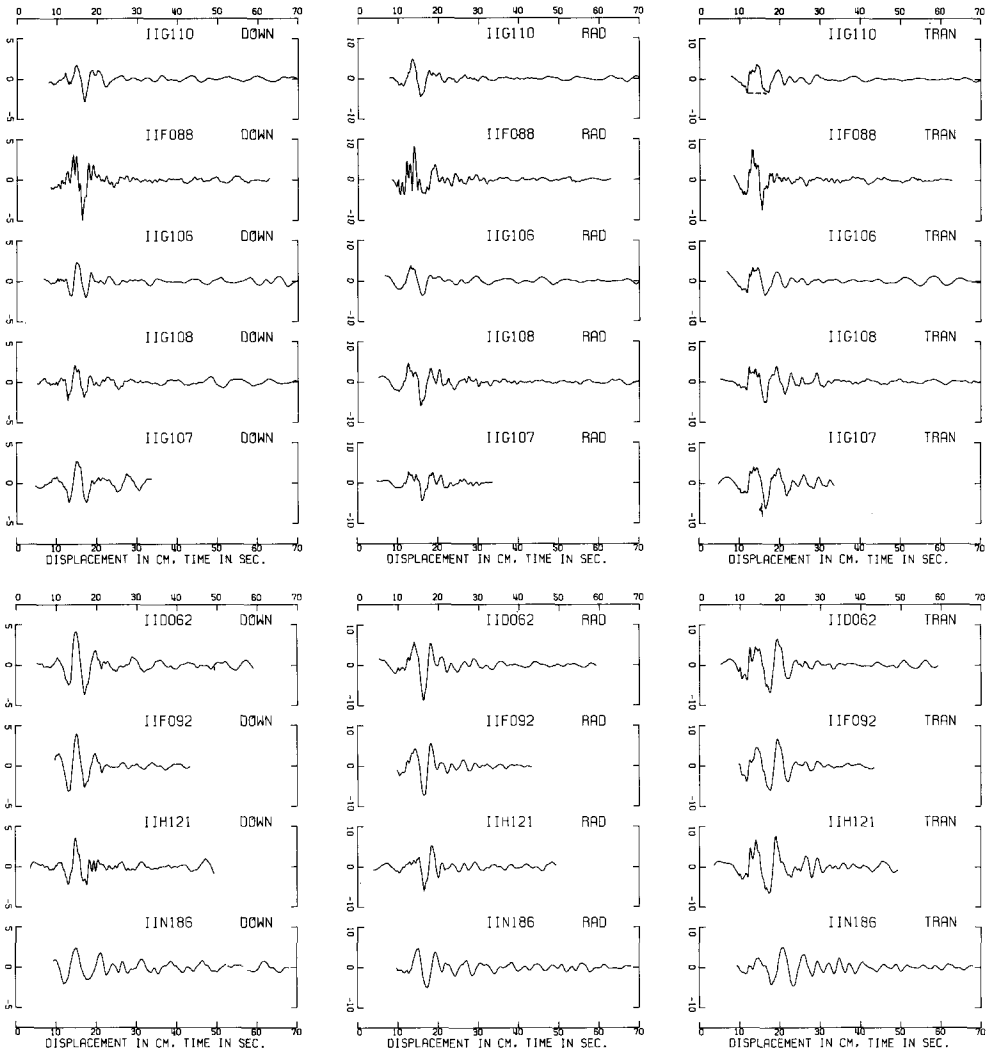

FIG. 10 A. Ground displacements along Profile 1.

tance. For the first five stations (G110, F088, G106, G108, and G107; $32 \leqq R \leqq 40$ km), $S!$ is followed in 1.5 to 2.0 sec by a large transverse displacement of 5 to 7 cm that is effected in 1 sec or less, accompanied by large particle velocities and accelerations. This motion is the initial rise of a transverse pulse of 4- to 5-sec duration. It is followed by a second pulse at approximately 17 sec. This secondary transverse pulse is more variable in amplitude and frequency content, but its amplitude generally grows with increasing epicentral distance. For $43 \leqq R \leqq 54$ km (D062, F092, H121, and N186), the amplitude of the secondary transverse pulse is dominant. At N186 ($R = 54$ km), the transverse

component of motion has the appearance of a dispersed Love wave. The ordering of arrivals according to decreasing period on the transverse component at N186 is well-developed, and much of the high-frequency component of the primary transverse pulse following *S*! is absent, either because of dispersion or material absorption.

The profile of transverse components in Figure 10A appears to be a nice example of how a transverse shear pulse at close ranges (G110) interacts with the Earth's surface

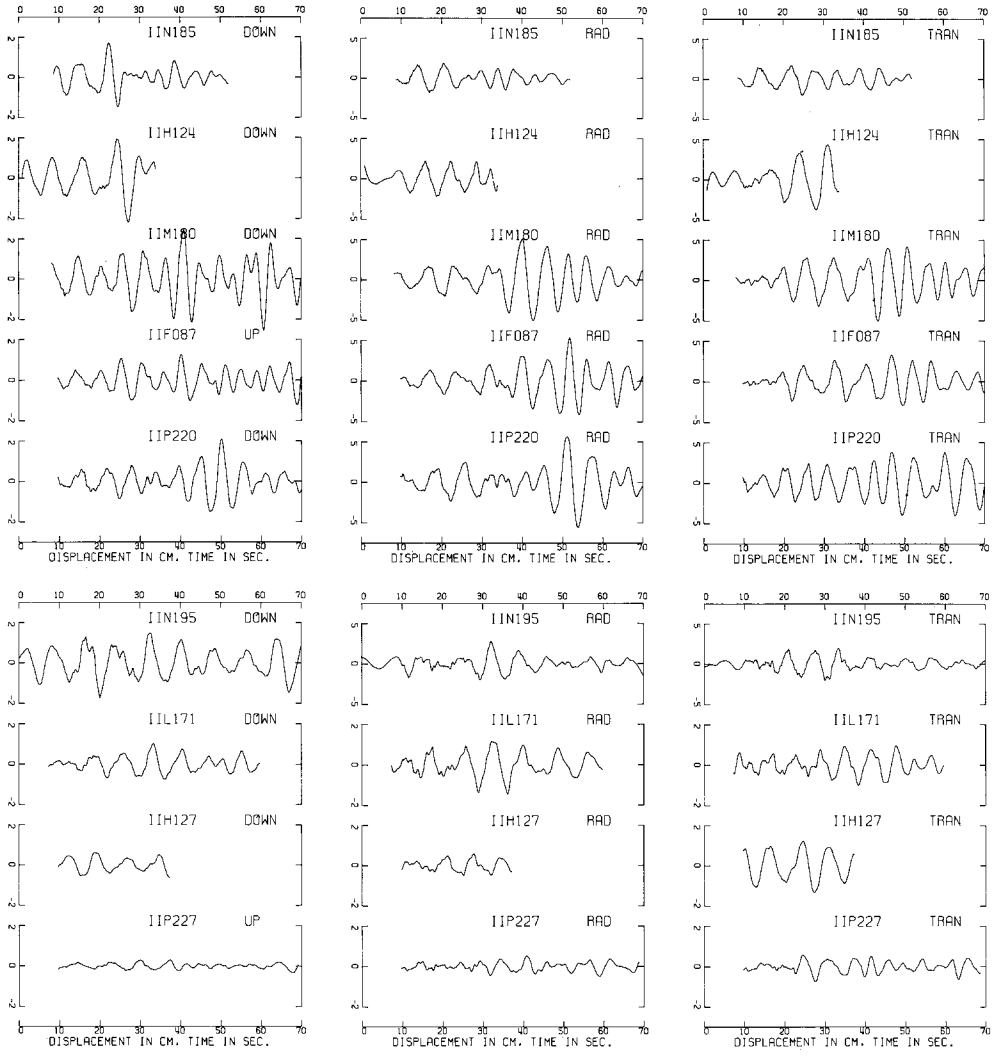

FIG. 10 B. Continuation of Profile 1.

to develop into a surface (Love) wave and subsequently disperses (N186). Much of the dispersion at N186 is presumably related to the wave form's traverse across the sedimentary cover in the San Gabriel Valley (Figure 1).

Station G110 is only 32 km from the epicenter, and the source-station path is almost entirely within the crystalline mass of the San Gabriel Mountains. Both effects should minimize the distortion of bodily shear pulses leaving the hypocentral region, and the transverse wave form at G110 is of minimum complexity relative to the other stations. Under the assumption that the primary transverse pulse at G110 is a far-field shear pulse,

we can estimate the seismic moment (M_o) and source dimension (r) of the event that generated it with the results of Brune (1970, 1971)

$$M_o = 4\pi\rho\beta^3 R(\Omega_o/0.85) \tag{1}$$

$$\tau\cdot(\beta/r) \approx 3. \tag{2}$$

In these relations, the density $\rho = 2.7$ gm/cm^3 and the shear velocity $\beta = 3.2$ km/sec; Ω_o is the time integral of the far-field shear pulse and τ is the pulse width in seconds. The factor of 0.85 in (1) corrects for free-surface reflection of SH waves, an average value of the radiation pattern, and the contribution from the perpendicular horizontal component.

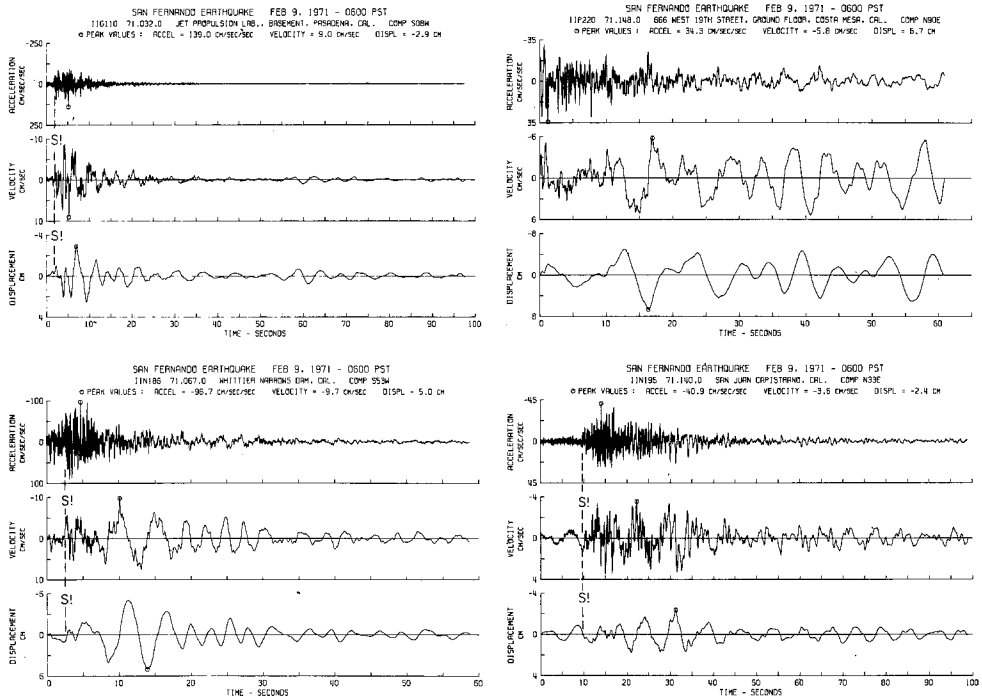

FIG. 11. Acceleration, velocity, and displacement for one component of ground motion at four sites of Profile 1 with the identification of $S!$. $S!$ is assumed to trigger the accelerograph at P220.

The portion of the transverse displacement at G110 isolated for consideration as a far-field shear pulse is indicated by the dashed line between 11 and 16 sec. The area between this dashed line and the transverse displacement is $\Omega_o = 35$ cm-sec; the pulse width is given by the length of the dashed line $\tau = 4.5$ sec. Then $M_o = 1.3\times10^{26}$ dyne-cm and $r = 5$ km. The M_o value compares reasonably well with that for the San Fernando earthquake, but r is about one-half the estimated source dimension of faulted area. Three separate investigations (Hanks, 1972, 1974; Trifunac, 1974; Alewine, 1974), however, have suggested that the San Fernando earthquake was initiated with massive, but relatively localized, faulting in the hypocentral area. In this region of initial rupture, these investigations have suggested that faulting distributed over dimensions of 3 to 6 km was accompanied by a seismic moment of $0.6\text{–}1.7\times10^{26}$ dyne-cm. The additional observation that the primary transverse pulse width is 4.5 sec but that the faulting duration was 8 (Hanks, 1972, 1974; Alewine, 1974) to 12 sec (Trifunac, 1974), suggests that the primary transverse pulse cannot represent the entire faulting mechanism but may

well represent the initial rupture event. The rise time of the primary transverse pulse at G110 compares favorably with the rise time of the equivalent shear pulse at Pacoima Dam (Hanks, 1972, 1974).

The dispersion that is indicated on the transverse component at N186 is also apparent on the vertical and radial components. Particle motion trajectories in the radial-vertical plane describe retrograde ellipses at N186 in the time interval of significant motion, approximately 10 to 25 sec. For these reasons, we interpret the vertical and radial components of ground displacement as largely consisting of dispersed Rayleigh waves. At closer ranges, displacements on the vertical and radial components are more pulse-like, but, in the sense that motion upward (for example, the peak on the vertical component at approximately 15 sec) correlates with motion toward the source (the negative radial direction), the vertically polarized shear pulses are Rayleigh pulses. As was the case for the transverse component, the vertical and radial components indicate the development of Rayleigh waves and their subsequent dispersion from a more simple, vertically polarized shear pulse observed at closer ranges.

Figure 10B is the continuation of Profile 1 for $75 \leqq R \leqq 222$ km. At stations N185 and H124, the primary transverse pulse arrives between 11 and 12 sec, but its amplitude has diminished considerably through geometrical spreading and the loss through dispersion of all but its longest period components. Beyond 76 km, it is no longer identifiable. The displacements at M180, F087, and P220 are dominated by 3- to 5-sec waves with amplitudes of 3 to 5 cm, generally larger displacements than those at the closer stations N185 and H124. Moreover, the duration of the latter three records is considerably greater (99, 82, and 61 sec for M180, F087, and P220, respectively). These three stations lie just southeast of the area of greatest depth to basement in the Los Angeles Basin (Figure 1), and it is likely that the displacements at M180, F087, and P220 reflect the presence of this structure, at least in part. There is some suggestion of phase coherence at these three stations, but the displacement records are complicated and *S*! was not identified at F087 and P220. It is unfortunate that no accelerographs were sited on this great sedimentary thickness at the time of the San Fernando earthquake.

At stations N195 and L171, identification of *S*! was again possible. At these distances, it corresponds to the shear arrival refracted from the Mohorovičić discontinuity, a more efficient propagation path than through the lower crust and then through the substantial thickness of sedimentary cover at F087 and P220, where it was not identified. The displacements in San Diego (H127 and P227, $R \simeq 220$ km) are at the noise level and are displayed primarily as a maximum estimate of ground displacement at this range.

Profile 2 (*Figure 12*). Profile 2 consists of eleven stations in a direction northwest from the epicenter, approximately 180° away from Profile 1. Source-station azimuths vary from N33W to N56W; epicentral distances range from 23 to 227 km. Station data for Profile 2 are presented in Table 3, and ground displacements are presented for these sites in Figure 12.

The most striking aspect of Profile 2 is simply the much weaker ground displacements relative to Profile 1 at comparable epicentral distances. *S*! could be identified at only three stations (J144, J143, and D056); it arrives at 0.8 sec in Figure 12. Indeed, all of the displacements beyond $R = 53$ km (station F104) are at or below the noise level of approximately 1 cm. At the four closest stations (J144, J143, D056, and F104), there is little if any phase correlation. With the exception of a few isolated peaks, ground displacements at even these four stations ($23 \leqq R \leqq 53$ km) are less than 2 cm. For $30 \leqq R \leqq 100$ km, displacement amplitudes along Profile 2 are lower by a factor of 3 to 10 than displacement amplitudes at comparable epicentral distances along Profile 1.

Figure 13 is the radiation pattern for 8-sec Rayleigh waves based on the source model

of Alewine (1974). This source model consists of four spatially and temporally separated point sources, arranged such that rupture initiates in the hypocentral region and propagates to the south at an effective rupture velocity of 3.2 km/sec. While details of the radiation pattern depend sensitively on the direction and velocity of rupture propagation, the amplification of Rayleigh-wave excitation in this period range at southern azimuths relative to northern azimuths can be recovered under a wide range of model parameters.

Superimposed on this radiation pattern are the intensity contours reported by Scott (1971) and the azimuth ranges of Profiles 1 to 4. As will be seen shortly, displacement amplitudes along Profile 1 are intermediate to those along Profile 3 and Profile 4, in the manner suggested by the radiation pattern. Also, a selection of ground displacements at northern azimuths suggest that the diminished amplitudes along Profile 2 are a general feature of the entire northern azimuth sector.

It is noteworthy that the higher levels of intensity (down through Intensity VI) are highly asymmetric about the epicenter, in a manner such that the same level of intensity is felt at much greater distances to the south of the epicenter than to the north of it. In a gross fashion, the observed azimuth variations of ground displacement amplitudes

TABLE 3

STATION DATA: PROFILE 2

EERL-CIT Ref. No.	Address and Location	Instrument	R (km)	φ (deg)
J144	Lake Hughes Array, station 12	AR-240	23	319
J143	Lake Hughes Array, station 9	AR-240	27	326
D056	Castaic, Old Ridge Route	AR-240	29	305
F104	Gorman, Oso Pumping Plant	AR-240	53	326
F102	Fort Tejon	AR-240	70	317
M179	Grapevine, Tehachapi Pumping Plant	AR-240	70	327
E071	Wheeler Ridge	AR-240	88	322
K153	Maricopa Array, station 1	RFT-250	119	304
P230	Buena Vista	AR-240	120	314
P225	Taft, Lincoln H.S. Tunnel	Standard	127	310
P229	Cholame–Shandon Array, station 8	AR-240	227	309

and the 8-sec Rayleigh-wave radiation pattern correlate well with the Intensity VI and VII contours.

The single point-source radiation pattern for Love waves is generally much different from that for Rayleigh waves, but the displacement data indicate that the transverse and radial displacement amplitudes are generally comparable at any azimuth. It therefore appears that variations in the general level of ground displacement are influenced primarily by source propagation, azimuthal variations in the gross geological structures, or some combination of both. Source propagation tends to distort both the Rayleigh and Love-wave single point-source radiation patterns in the same way, and indeed, the strong north-south asymmetry of the 8-sec Rayleigh-wave radiation pattern of Figure 13 is primarily a function of source propagation from north to south. Coincidentally, the great thicknesses of low-velocity sediments in the Los Angeles Basin south and southeast of the epicenter will tend to amplify ground motion in this period range at these azimuths, resulting in amplitude variations comparable to those generated by the effects of source propagation. The absence of data in much of the eastern and western sectors precludes an assessment of the relative contribution of the two effects. Whatever the relative contribution of these two effects may be, it is still true that the higher intensity contours

correlate well with azimuthal variations in the general amplitude level of ground displacement, a surprising result in view of the general agreement that the higher intensity levels are based on the amplitude of high frequency ($\gtrsim$ 1 Hz) ground motion.

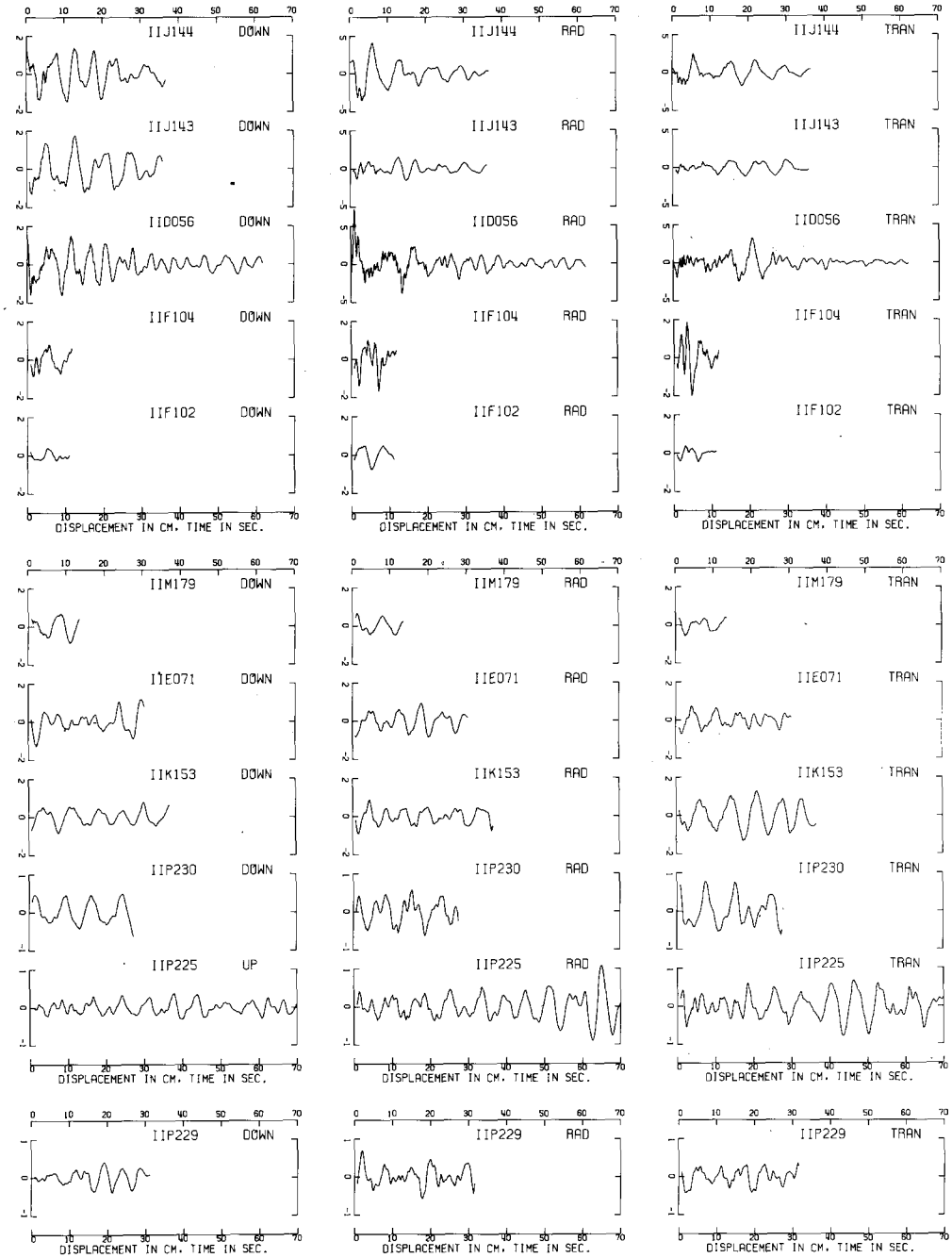

FIG. 12. Ground displacements along Profile 2.

Profile 3 (*Figure 14*). Profile 3 consists of eight stations in a direction east-southeast from the epicenter. Source-station azimuths vary from 108° to 125°, approximately 30° counterclockwise from Profile 1; epicentral distances range from 43 to 227 km. Station

data for Profile 3 are presented in Table 4, and ground displacements for these sites are presented in Figure 14.

The phase *S*! has been identified at all stations but N197, although it is questionable at I140. In Figure 14, it arrives at 8.3 sec. A confirmed misidentification of horizontal

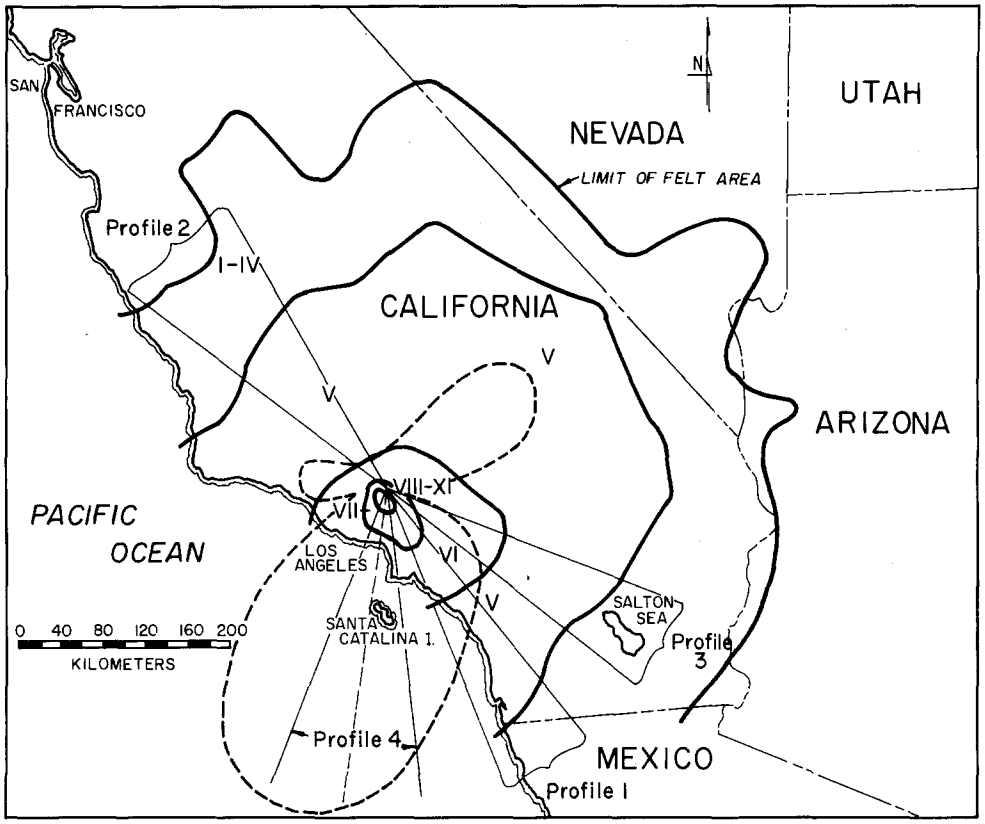

FIG. 13. A radiation pattern for 8-sec Rayleigh waves (dashed curve), the isoseismal contours of Scott (1971) (solid curves), and the azimuthal ranges of Profiles 1, 2, 3, and 4.

TABLE 4

STATION DATA: PROFILE 3

EERL-CIT Ref. No.	Address and Location	Instrument	R (km)	φ (deg)
P221	Arcadia, Santa Anita Reservoir	AR-240	43	125
P223	San Dimas, Puddingstone Reservoir	AR-240	65	123
N187	Upland, San Antonio Dam	RFT-250	72	112
F101	Colton	Standard	107	111
O206	San Bernardino, Hall of Records	RFT-250	109	108
O210	Hemet, Fire Station	RFT-250	151	120
N197	Anza, Post Office	RFT-250	186	120
J140	Borrego Springs, Fire Station	RFT-250	227	124

components at N187 necessitated the interchange (with a negative sign) of the components labeled RAD and TRANS such that radial displacement at N187 is along the positive ordinate in the second column. Similarly, transverse displacement at N187 is along the positive ordinate in the third column.

On the transverse component there is fairly good phase correlation between 8 and 20 sec at P221, P223, and N187; although the record is short at F101, it indicates that this phase correlation exists to this station (R = 107 km). The positive transverse motion beginning at approximately 8 sec is equated with the primary transverse pulse observed along Profile 1, although in a mildly dispersed form at even the closest station (R = 43 km). Its amplitude decreases from about 4 cm at P221 (R = 43 km) to less than 1 cm at F101 (R = 107). The amplitudes of transverse ground displacements along Profile 3

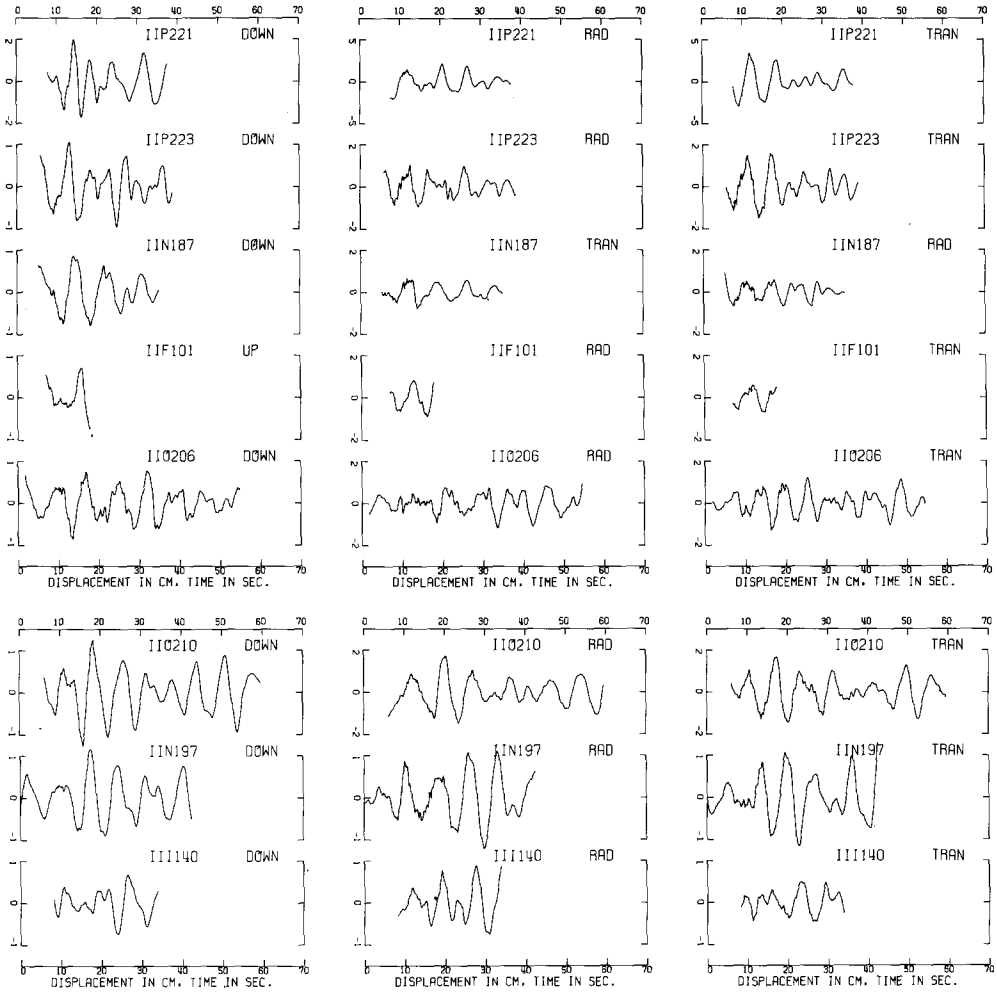

FIG. 14. Ground displacements along Profile 3.

are less than along Profile 1, but generally greater than along Profile 2 at comparable epicentral distances.

Phase correlation on the radial and vertical components is by and large confined to the single positive pulse between 10 and approximately 15 sec. Amplitudes on the radial component are generally less than on the transverse component. Radial and vertical components of displacement along Profile 3 are, however, somewhat greater than along Profile 2 at comparable epicentral distances, in agreement with the 8-sec Rayleigh-wave radiation pattern (Figure 13). The appearance of phase correlation on all components through F101 suggests that the noise level is something less than 1 cm. The absence of pronounced dispersion at P221, P223, and N187 of the sort noticed at N186 (Profile 1) is

presumably related to the fact that almost all of the three source-station paths are within the more uniform basement complex of the San Gabriel Mountains (Figure 1).

Profile 4 (*Figure 15*). Profile 4 consists of 11 stations in a direction south from the epicenter. Source-station azimuths vary from 168° to 199°, although this range is only $168 \leqq \varphi \leqq 185°$ with the exclusion of C048, J145, and H115. Epicentral distances range from 9 to 68 km. Station data for Profile 4 are presented in Table 5 and ground displacements for these sites are presented in Figure 15. The phase *S*! has been identified on all records and arrives at 6.2 sec in Figure 15.

The ground displacements beginning with station L166 ($R = 30$ km) and at greater epicentral distances are structurally akin to those discussed previously for Profile 1 at $30 \lesssim R \lesssim 70$ km; that is, relatively concise Rayleigh and transverse pulses develop into surface waves and subsequently disperse. The dispersion, however, is very strong, and the main energy group between 10 and 20 sec at D068 is delayed considerably for even modest increases in epicentral distances. Even more interesting is the *growth* of the displacement amplitudes for this group with increasing epicentral distance in the range

TABLE 5

STATION DATA: PROFILE 4

EERL-CIT Ref. No.	Address and Location	Instrument	R (km)	φ (deg)
C041	Pacoima Dam	AR-240	9	180
C048	Los Angeles, 8244 Orion, 1st fl.	AR-240	22	199
J145	Los Angeles, 15107 Van Owen, bsmt.	RFT-250	24	197
H115	Los Angeles, 15250 Ventura, bsmt.	SMA-1	30	194
L166	Los Angeles, 3838 Lankershim, bsmt.	RFT-250	30	170
D068	Los Angeles, 7080 Hollywood, bsmt.	AR-240	35	168
D057	Los Angeles, Hollywood Storage Bldg., bsmt.	Standard	37	168
S262	Los Angeles, 5900 Wilshire, "B" Pkg. lot	MO-2	39	172
H118	Los Angeles, 8639 Lincoln, bsmt.	RFT-250	50	185
S267	Los Angeles, 5260 Century, 1st fl.	MO-2	51	174
N191	Palos Verdes Estates, 2516 Via Tejon	RFT-250	68	176

$30 \leqq R \leqq 39$ km (L166, D068, D057, and S262). That the displacement wave forms at S262 (the site of greatest displacements beyond L166) are not a function of local site conditions or artifacts of the data processing may be verified by their comparison with those in Area 1, located approximately $3\frac{1}{2}$ km to the east of S262. As was noted previously the displacements wave forms of Area 1 agree in gross fashion with those in Area 2, located still another 3 to 4 km east-southeast of Area 1. For distances greater than that of S262 ($R = 39$ km), amplitudes diminish with increasing distance, with increasing delays of the main energy group.

At close epicentral distances, the growth of surface-wave amplitudes over a limited range of epicentral distances is not an unexpected result, although it does require special circumstances of the propagational medium and the source-station geometry. In this connection, it may be noted that the depth to basement increases precipitously in progressing southward from D068 (Figure 1) and that radiation with wavelengths comparable to the depth to basement can be expected to be amplified accordingly; moreover this wavelength increases in passing from D068 to S262. This observation may also account for the strong dispersion between L166 and S267 ($R = 51$ km).

The stations C048, J145, and H115 ($22 \leqq R \leqq 30$ km) are in the azimuth range $194 \leqq \varphi \leqq 199°$, approximately 20° clockwise from the azimuths of the stations discussed

previously .There is little coherence in ground displacements between these three stations and the stations beginning with L166, suggesting that the local structure of the San Fernando Valley has had a significant effect on the ground motion recorded at C048,

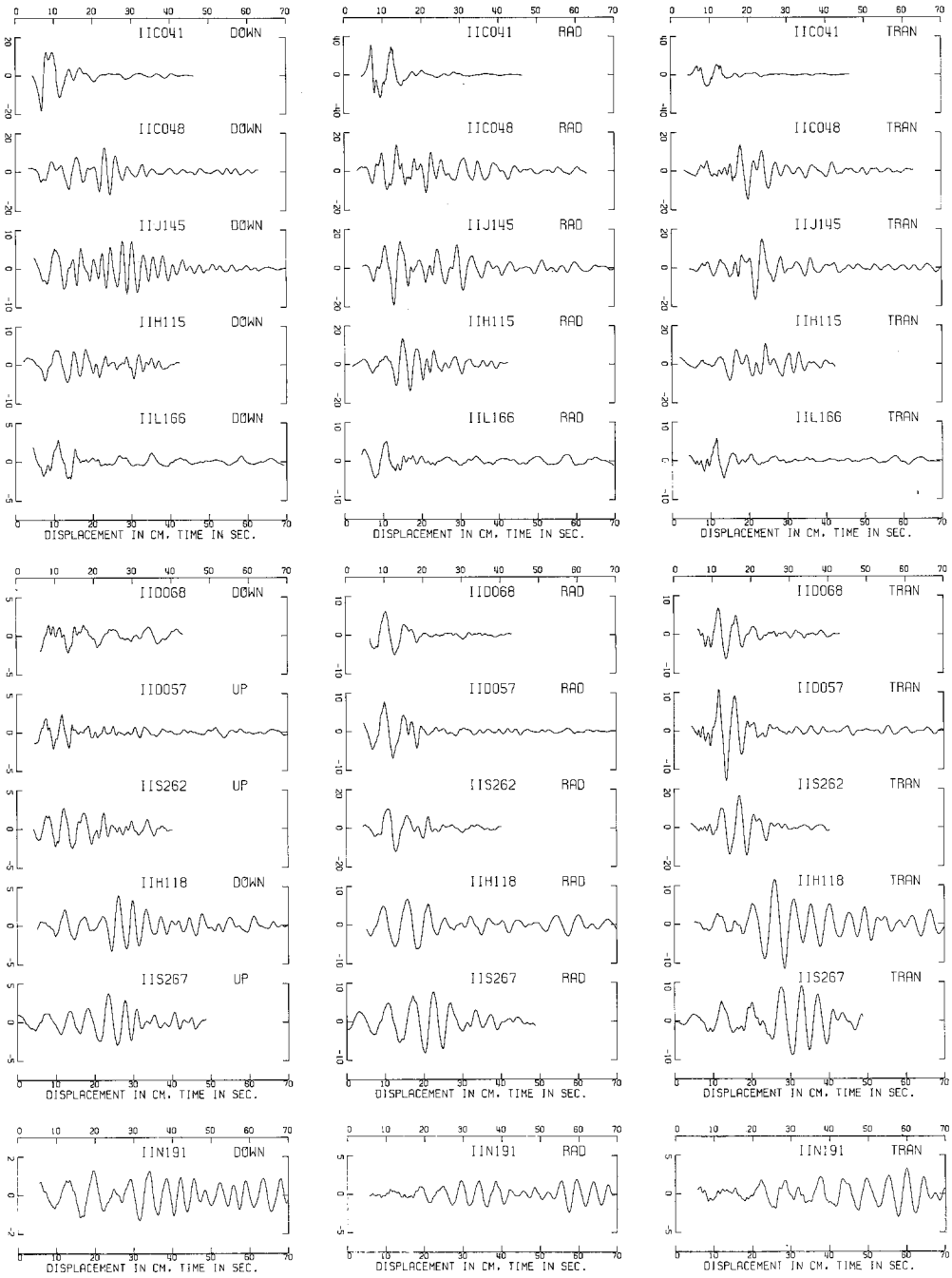

FIG. 15. Ground displacements along Profile 4.

J145, and H115. The coherence between C048, J145, and H115 is fair, but generally these records are complicated.

The amplitudes of ground displacement at epicentral distances $30 \lesssim R \lesssim 70$ km

are generally larger than those at comparable epicentral distances along Profile 1. At $R \simeq 40$ km (S262 on Profile 4, F092 on Profile 1), this difference in excitation is almost by a factor of 2. This difference in excitation is suggested by the radiation pattern in Figure 13, but as we have seen earlier, much of it may be related to the local structure of the Los Angeles Basin.

TABLE 6

STATION DATA: NORTHERN AZIMUTHS

EERL-CIT Ref. No.	Address and Location	Instrument	R (km)	φ (deg)
F103	Pearblossom	AR-240	46	76
G114	Palmdale	RFT-250	33	55
O207	Fairmont Reservoir	Standard	33	351
J141	Lake Hughes Array, station 1	AR-240	30	349
J142	Lake Hughes Array, station 4	RFT-250	27	342
E081	Piru, Santa Felicia Dam	AR-240	33	280

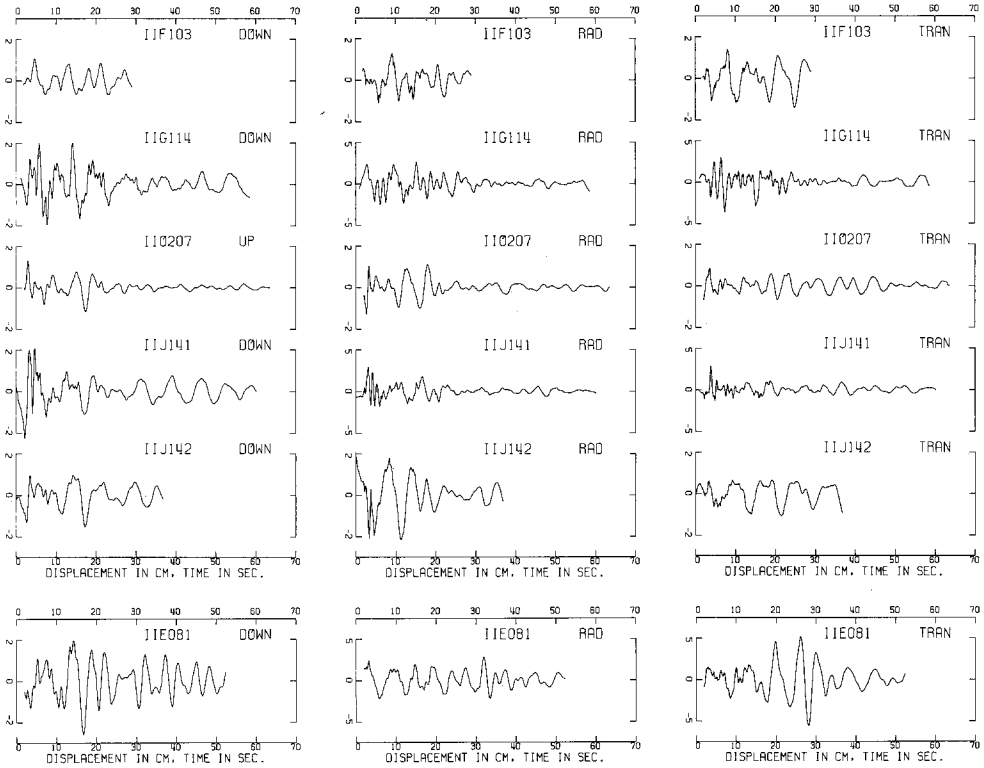

FIG. 16. Ground displacements for selected sites of the northern sector.

Northern azimuths (*Figure 16*). To sample ground displacements in the northern azimuth sector more completely, six stations at $27 \leqq R \leqq 46$ km have been chosen for $-80° \leqq \varphi \leqq 76°$. Data for these stations are presented in Table 6 and vertical, radial, and transverse components of ground displacements at these sites are presented in Figure 16. The general conclusion to be drawn from Figure 16 is that the amplitudes of ground displacement in this range of epicentral distances are generally small throughout

the northern sector, relative to displacement amplitudes at comparable epicentral distances in the southern azimuth sector (Profiles 1, 3, and 4). With the exception of E081 and isolated peaks at the other sites, displacement amplitudes are less than 2 cm, indicating that the diminished displacement amplitudes along Profile 2 are not confined to a localized azimuthal range.

The Rayleigh-wave radiation pattern of Figure 13 has a localized maximum at $30° \leqq \varphi \leqq 70°$, wherein radial and vertical displacements might be expected to be comparable to those along Profile 1 at similar epicentral distances. G114 is at $\varphi = 55°$, $R = 33$ km. Although the amplitudes of radial displacement at G114 are generally larger than elsewhere in the northern sector, in qualitative agreement with the relative excitation implied by Figure 13 for the northern sector, they are only about one-half of those at G110 ($\varphi = 137°$, $R = 32$ km) on Profile 1.

Conclusions

The broadcast significance of this investigation stems from the essential simplicity of the ground displacement wave forms generated by the San Fernando, California, earthquake. Within limited ranges of epicentral distance and source-station azimuths, ground displacements display strong coherence. Across broader variations of R and φ, many of the observed variations in the displacement wave forms are easily attributable to well-understood seismological phenomena. The concepts and parameters of seismic moment, source dimension, radiation pattern, rupture propagation, the development of surface waves and their subsequent dispersion, and azimuthal variations of geological structure are all reflected in the gross amplitude and frequency content of the displacement wave forms and their observed variations with epicentral distance and azimuth. While the ground displacements exhibit a complexity well beyond this interpretive framework, these complexities more likely reflect poorly understood details of the source mechanism and propagation paths than its basic inadequacy.

As such, there is considerable optimism that numerical synthesis of these data using already known source parameters and crustal structures of only moderate complexity can reproduce much of the gross amplitude and frequency content of the observed ground displacements and, with further refinement, can proceed to elucidate details of the displacement wave form; these efforts are now in progress. A major impediment to these efforts is the absence of absolute time information, which appreciably restricts the full seismological significance of these observations. Strong-motion accelerographs with the capability of writing the WWVB ratio time code directly on the recording medium are now commercially available and have been deployed in several areas of California (Dielman *et al.*, 1975). Such a capability for the observations presented here would have obviated the necessity for temporal alignment based on *S*!, with its associated uncertainties, and would have yielded direct information on crustal structure as well, which presently can only be inferred. Such information seems well worth the nominal increase in cost above the basic instrumental package.

The routine analysis procedures applied by the Earthquake Engineering Research Laboratory of the California Institute of Technology are capable of extracting long-period data from strong-motion accelerograms with considerable accuracy. For a data sensitivity of approximately 7.6 cm/g, uncertainties in displacement are approximately 0.5 to 1 cm in the period range 5 to 8 sec, 1 to 2 cm at periods near 10 sec, and several (2 to 4) centimeters in the 10- to 15-sec period range. Both the absolute values and the trend of increasing uncertainty with increasing period are in accord with the expectations of Trifunac *et al.* (1973b) for this sensitivity. The spurious 11-sec disturbance arose

fundamentally from data-processing techniques (Hanks, 1973), is easily avoidable, and does not reflect basic instrumental inadequacies. The choice of $f_{LC} = 0.125$ Hz was a convenient expedient for the data considered here, but it is not a fundamental choice. Particularly for larger earthquakes, for which amplitudes of ground displacement are correspondingly larger, longer-period information can and should be admitted, with no degradation of signal-to-noise quality.

Concomitant to an improved understanding of the generation and propagation of long-period strong ground motion will be a more realistic appraisal of design earthquakes within this frequency band. Given the considerable economic investment in and potential seismic hazard of modern long-period structures, refined estimates of long-period strong ground motion and their consequent implications for aseismic design criteria are likely to be the most significant results of this investigation.

Acknowledgments

I appreciate the efforts of Joseph Galvan, Vincent Lee, Laszlo Lenches, James Justiss, Barbara Turner, and Sharon Vedrode in various stages of data manipulation and manuscript preparation. D. E. Hudson, G. W. Housner, and M. D. Trifunac have offered valuable comments during several phases of this investigation. C. R. Allen, H. Kanamori, R. B. Matthiesen, and O. W. Nuttli critically read the manuscript. This research was supported in part by the National Science Foundation, the Earthquake Research Affiliates Program of the California Institute of Technology, and the Advanced Research Projects Agency of the Department of Defense, as monitored by Air Force Office of Scientific Research under contract F44620–72–C–0078.

References

Alewine, R. W. (1974). Application of linear inversion theory toward the estimation of seismic source parameters, *Ph.D. Thesis*, California Institute of Technology, Pasadena, 303 pp.

Allen, C. R., T. C. Hanks, and J. H. Whitcomb (1973). Seismological studies of the San Fernando earthquake and their tectonics implications, *Calif. Div. Mines and Geol. Bull.* 196, (in press).

Brune, J. N. (1970). Tectonic stress and the spectra of seismic shear waves, *J. Geophys. Res.* **75,** 4997–5009.

Brune, J. N. (1971). Correction, *J. Geophys. Res.* **76,** 5002.

Dielman, R. J., T. C. Hanks, and M. D. Trifunac (1975). An array of strong-motion accelerographs in Bear Valley, California, *Bull. Seism. Soc. Am.* **65,** 1–12

Hanks, T. C. (1972). A contribution to the determination and interpretation of seismic source parameters, *Ph.D. Thesis*, California Institute of Technology, Pasadena, 184 pp.

Hanks, T. C. (1973). Current assessment of long-period errors, in Strong Motion Earthquake Accelerograms—Volume IIG, M. D. Trifunac, A. G. Brady, and D. E. Hudson, *Earthquake Engineering Research Laboratory, EERL 73–52*, California Institute of Technology, Pasadena.

Hanks, T. C. (1974). The faulting mechanism of the San Fernando earthquake, *J. Geophys. Res.* **79,** 1215–1229.

Lee, A. M. (1932). The effect of geological structure upon microseismic disturbance, *Monthly Notices Roy. Astron. Soc.* **3,** 83–105.

Scott, N. H. (1971). Preliminary report on felt area and intensity, *U.S. Geol. Surv. Profess. Papers* **733,** 153–154.

Trifunac, M. D. (1970). Low-frequency digitization errors and a new method for zero base-line correction of strong-motion accelerograms, *Earthquake Engineering Research Laboratory, EERL 70–07*, California Institute of Technology, Pasadena.

Trifunac, M. D. (1971). Introduction to Volume II, in Strong Motion Earthquake Accelerograms—Volume IIA, D. E. Hudson and A. G. Brady, *Earthquake Engineering Research Laboratory, EERL 71–50*, California Institute of Technology, Pasadena.

Trifunac, M. D., A. G. Brady, and D. E. Hudson (1973a). Strong motion earthquake accelerograms, Volume IIG, *Earthquake Engineering Research Laboratory, EERL 73–52*, California Institute of Technology, Pasadena.

Trifunac, M. D., F. E. Udwadia, and A. G. Brady (1973b). Analysis of errors in digitized strong-motion accelerograms, *Bull. Seism. Soc. Am.* **63,** 157–187.

Trifunac, M. D. (1974). A three-dimensional dislocation model for the San Fernando, California, earthquake of February 9, 1971, *Bull. Seism. Soc. Am.* **64**, 149–172.

EARTHQUAKE ENGINEERING RESEARCH LABORATORY
SEISMOLOGICAL LABORATORY
CALIFORNIA INSTITUTE OF TECHNOLOGY
PASADENA, CALIFORNIA 91109
DIVISION OF GEOLOGICAL AND PLANETARY SCIENCE
CALIFORNIA INSTITUTE OF TECHNOLOGY
CONTRIBUTION NO. 2473.

Manuscript received May 9, 1974.